MODELING AND IDENTIFICATION OF THERMALLY ACTUATED MICRO-ROBOTS

by

SAI KALYAN YELIKE

Presented to the Faculty of the Graduate School of
The University of Texas at Arlington in Partial Fulfillment
of the Requirements
for the Degree of

MASTER OF SCIENCE IN ELECTRICAL ENGINEERING

THE UNIVERSITY OF TEXAS AT ARLINGTON
August 2012

ACKNOWLEDGEMENTS

I would like to thank my supervising professor Dan O. Popa for constantly motivation and encouraging me, and also for his valuable advice during the course of my studies. I would like to thank Michael T. Manry and Kamesh Subba Rao for their interest in my research and for taking time to serve in my thesis committee.

I would like to extend my appreciation to my colleagues Mohammed Rashid Pac, Rakesh Murthy and Isura Ranatunga for their support during my thesis work.

Finally, I would like to extend my deep gratitude to my cousin Kandula Vijay Gopal Yadav for his valuable support during my graduation program. I'm sincerely thankful to my parents who have encouraged, motivated me and sponsored my graduate studies. I wish to thank all my friends who have helped me during my graduate studies.

July 20, 2012

ABSTRACT

MODELING AND IDENTIFICATION

OF THERMALLY ACTUATED

MICRO-ROBOTS

Sai Kalyan Yelike, M.S.

The University of Texas at Arlington, 2012

Supervising Professor: Dan O. Popa

This thesis explains the system identification of thermally actuated micro-robots and actuators developed at UTA-NGS (Next Generation Systems) and ARRI (Automation Robotics Research Institute). The energy used to power these actuators are externally-supplied voltage and class IV Laser sources. The micro-robots actuated with class IV laser sources have displacements recorded through a camera. Applied laser input waveforms and micro-robot's positional displacement are used for system identification of the Micro-robot. Various system identification methods (non-recursive and recursive) are used for creating a mathematical model of the physical system (Micro-robot).

A similar approach is followed for micro-actuators known as chevron actuators powered by externally controlled voltage sources. The micro-actuator displacements are measured through optical interferometer techniques, and the applied input voltage sources properties and displacements are used for system identification..

Finally, system identification is performed to find the relation to the externally applied voltage source and force generated by the actuators. A force sensor with micro precision is

used to measure the force generated by the actuators. Applied input voltage source and measured force sensor are used for system identification of the actuators. Both recursive and non-recursive methods are used for system identification of the micro-actuators.

TABLE OF CONTENTS

LIST OF ILLUSTRATIONS

Figure Page

CHAPTER 1

INTRODUCTION

1.1 Motivation for working with micro-robots

Micro-robots are of great interest to the future of technology, particularly in areas such as micro and nano manufacturing.. The small size of these robots could potentially play an important role in many other applications, such as medical, biotechnology, defense, etc. These micro-robots may be self-powered running on internally stored energy such as batteries, etc. There are other robots which are powered or actuated externally using sources like solar energy, vibration, magnetic, laser, voltage supply, etc. The externally supplied energy is converted into a different energy form internally, which is further used in actuating the micro-robots desired motion. Many journals and papers have been dedicated to the definitions of micro-actuators and micro-robots. An encyclopedic classification of micro-actuators was specified by Popa in [1].

Some micro-robots are made of single or multiple micro-actuators depending on the required degrees of freedom and type of application. In [8], Loizou and Kyriakopoulos discussed one such micro-robot driven by piezo-electric actuation which propels on the principle of stick and slip in addition with navigation equations, a collision avoidance path following control has been developed. In this thesis, we will be discussing micro-robots which are actuated externally with the help of laser and voltage sources. This externally supplied source is internally converted into thermal energy which produces the desired motion or actuation depending on the application. The main aspect of working with micro-robots is to apply them for specific task which involves controlling them. In [18], Gensler et., al. discuss about a MEMS-based Implantable drug delivery system with reservoir and silicon pump used for therapeutic applications like chemotherapy. With telemetry, a wireless mode for recharging, tuning and

monitoring the device was proposed. Many papers and articles have been dedicated for designing and modeling the micro-grippers, a comprehensive discussion of electro-thermal modeling of a thermally actuated micro-grippers is proposed in [17] by Mayyas et. al.,. A four degree of freedom micro-robot used for considerable force generation is proposed in [12] which will be applied for different applications.

Controlling a system requires to understand the nature of the system in terms of it characteristic relation between its input and output. As this thesis may be the future reference for control systems application to micro-robots, we will be discussing about system identification methods for micro-robots and micro-actuators. Since the micro-robots are manufactured from micro-actuators, we will be spending more effort in understanding their nature.

In this work we have performed several experiments on the micro-robots which are actuated using laser source and micro-actuators called chevrons which are actuated with laser and electro-voltage. The measurements from these experiments were recorded and rearranged to apply system identification techniques leading to system models. There are a number of function models available which may be an appropriate fit to the experimental data. In this thesis, we employ models which are commonly applied to control systems applications using adaptive and non-adaptive methods. The subsection below gives an overview of system identification procedures and applications to different problems.

1.2 Overview of Modeling & System Identification Techniques

Modeling and System identification is a multidisciplinary field which can be used across a wide range of systems or processes in identifying the characteristics of any system whose precise nature are difficult to derive and model. Whether the system exhibits linear or non-linear characteristics, with sufficient amount of measurement data, approximate models of the system can be identified from a set of template models.

Systems whose physical characteristics are hard to model or derive are called black box models. These systems do not possess a particular mathematical model either partially or completely. Only the number of inputs that can be applied and number of outputs that can be obtained are the only information known about the system. The internal state variables may be linearly or non-linearly related to the input and output variables, or the system may be badly affected by the noise from the external or internal source. A comprehensive description of the system identification techniques is given in [29] by Ljung. All these properties are to be accounted for in identifying a precise model to the system. For modeling and identification of such systems require a rigorous set of inputs encompassing the entire range of frequency bandwidth need to be applied to the system. It would be an added advantage if the input range limits and bandwidth are known in advance, which would further simplify the input design process covering entire bandwidths. The measurement dataset can be broken into two sets called modeling data and validation (or verification) data. The measurement data is used for system identification purpose while the validation data is used to validate or authenticate the identified model.

Different pre-built linear and non-linear template models with parameters are available, adjusting these parameters enhances the convergence rate of the given template model to the original plant model. These template model structures vary in complexity depending on the flexibility needed to encompass all the dynamics and noise characteristics of the system. Black-Box modeling is a trial and error based process, where the parameters of the trial and error based models are estimated from the measurement data and compared with the validation results. Söderström and Stoica in [30] give a description of system identification with primary focus on linear and non-linear least squares models and curve fittings.

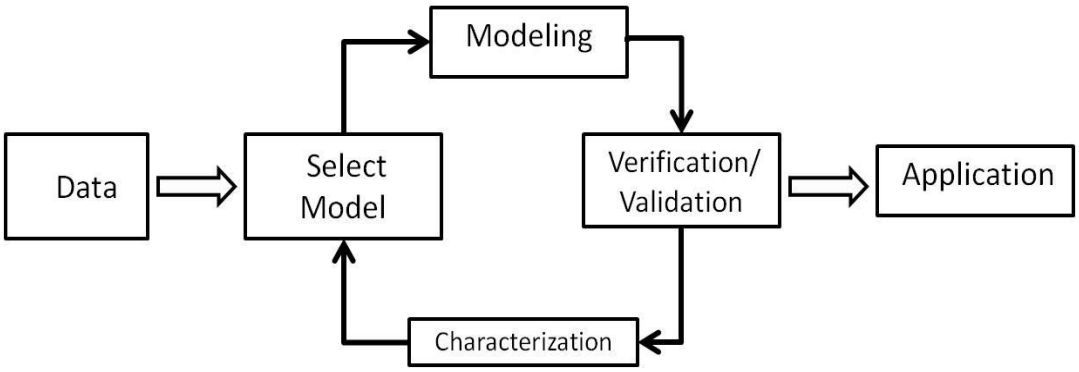

Figure 1.1 Generic System Identification work flow (courtesy: Wikipedia)

On the other hand, the Grey-box modeling is a method where the system needs to be modeled with a partial mathematical knowledge. As mentioned above for black box modeling, similar modeling principles also applies to grey box modeling accompanied by the partial mathematical knowledge. The mathematical relation among input and output variables can be obtained from observing the obtained input and output data accompanied by prior knowledge of system characteristics. The main aspects of process noise due to uncertainties in system behavior are dealt with by explicitly modeling the noise characteristics of the system. It always helps if the noise characteristics are specified prior to identifying the model, to speed up the system identification with minimal data sets or else more data sets are needed to identify the unknown noise characteristics. Many papers have been written in this particular field for microsystems applications.

The input data used for system identification can be provided in time domain or frequency domain. Correspondingly, template models which accept time domain or frequency domain data for modeling are available. Likewise, template models with linear input-output polynomial orders, state-space models, linear time-series models, non-linear ARX models, Hammerstein-Weiner models, etc. are available. Various books are available discussing the methods of modeling and identification, Ljung and Gold in [28] discuss about the system identification and physical modeling of dynamic systems, Ljung in [29], Soderstrom and Stoica in [30] are an excellent source of reference for system identification theory and algorithms.

For data available in frequency domain Pintelon and Schoukens [31] explain the identification techniques in frequency domain. Similarly, for non-linear systems Nelles in [32] discuss about the linear and non-linear state space modeling methods including numerical optimization techniques, neural network modeling approach.

Several papers have been dedicated to the modeling and identification for micro-systems for various applications. In [19], Popa discusses generating input profiles to MEMS actuators for identified reduced order model for input shaping to replace the Finite Element methods. In [3], a new modeling approach for complex MEMS devices based the number of bodies and number of constraints is proposed by Popa for rigid multi body dynamics.

System identification plays an important role in Control design for any black box or grey-box systems to produce a desired output response. In conjunction with the physical micro-robotic systems, mathematical equations describing the behavior of the some devices are available and with grey-box modeling techniques a complete identified system can be derived. While some devices which do not posses characteristic mathematical equations, black-box techniques are employed to characterize the system.

The application of control systems for micro-electromechanical systems has been discussed in [4] by Bryzek et. al,. In [5], a dynamic state space model for control of thermal MEMS Devices has been discussed by Borovic et. al., which contains the procedure for deriving a lumped dynamical state space model for MEMS devices that can be used for feedback control system application is derived in conjunction with FEA methods for deriving the unknown parameter values using system identification. A comprehensive discussion of different open and closed loop control strategies for optical MEMS devices has been discussed in [6], focusing on the dynamics of microscopic systems, control algorithms used and problems with the sensor failures are clearly specified. A ferrous material based micro-robot manufactured from multiple elements was described in [22] by Floyd et. al., which could be controlled by five macro-scale

magnets on uneven terrain with rugged properties. These types of robots play an important role in under fluid operations, micro assembly and micro manipulation.

1.3 Future scope of thesis application

Many micro-robots are manufactured from single or combination of multiple micro-actuators. Each micro-robot has its specific design depending on the type of application and the manufacturing methodology. In order to design these micro-robots, a thorough understanding of the micro-actuators which make up the micro-robot is very important. The figure below (fig. 1.2) shows a hypothetical micro-robot manufactured from multiple micro-actuator legs.

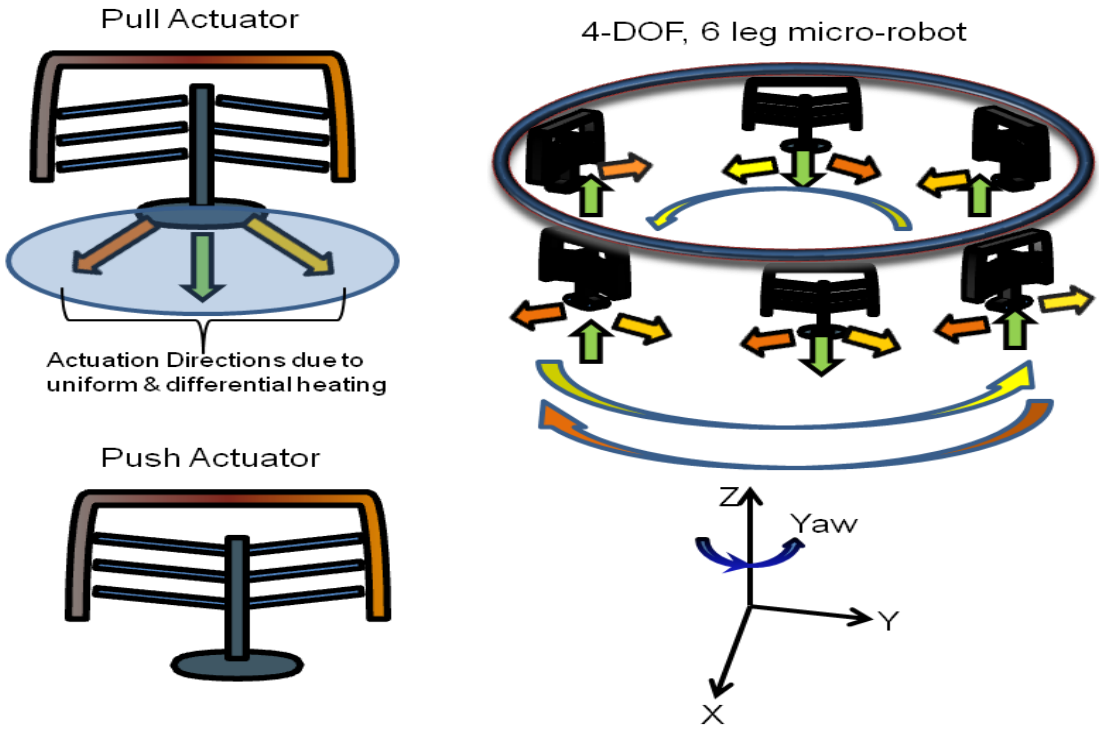

Figure 1.2 Futuristic hypothetical micro-robot made from multiple micro-actuators

In the above figure (fig. 1.2), the micro-robot manufactured from multiple chevron type micro-actuators. Each of these chevron type actuators are manufactured with differential heat distribution properties. Uniform heat distribution across the volume of the actuator results in

normal displacement of the shuttle leg shown in green colored arrows, while non-uniform heat distribution results in differential displacement of the shuttle leg resulting in rotation actuation motion. This differential displacement of the chevron leg is shown in orange and yellow colors.

The main idea of this hypothetical micro-robot is to provide four degree of freedom of motion which can perform complex maneuvers. Many other factors are taken into consideration for designing this micro-robot such as stability, mobility and sharp response times. The actuation source can be from a laser source or external voltage supply which finally converts to thermal energy generation.

The main challenge in designing a micro-robot is to understand the mathematical equations that define the characteristics of the micro-robot system. The entire micro-robot is a combination or integration of multiple chevron type actuators as shown in the above figure (fig. 1.2). Understanding the characteristic equations defining the chevron actuators is the prime step in designing these complicated micro-robots.

In this thesis, we will be discussing about these types of micro-actuators called chevrons which may are actuated with laser and voltage sources which in turn converts into thermal energy. We derive some standard ARX and ARMAX models to identify the relationship between the applied inputs and the corresponding actuation in terms of displacement and force generated. This thesis will be a source of guide for designing future micro-robots with multiple chevron type actuators. The numbers and equations specified may not be accurate in defining the precise characteristic of actuators as the properties of actuators varies with conditions.

1.4 Challenges in Modeling & System Identification of micro-robots

1) Designing micro-robots:

The process of designing micro-robot required the desired stick and slip motion characteristics. Physical properties of the raw material used for manufacturing these robots define its characteristic response to thermal input and bandwidth. A mass-spring damper

system with external force applied is the basic idea in design, where the actuation principle is the laser input source via heat generated. In [15], Kole et. al., discuss on MEMS based in-place Micro-pumps used for biotechnology applications for drug delivery, cell manipulation made from micro-actuators with electro-thermal actuation. A comprehensive discussion of concepts with experiments for micro positioning, micro handing and micro assembly of MEMS components was discussed in [21] by Bou, Almansa-Martin with funding from European Commission. In [20], an electro statically actuated diagraph is used for controlling the flow of fluid in a micro-pump with an external voltage source by Saif et. al., . An analytical model is used for predicting the state of the pump at operating set points which has non-linear elasto-electro-hydrodynamic behavior.

In conjunction with appropriate shaping and dimples placement in order to generate stick motion in one direction while slipping in the reverse direction, a complete modeling of the entire system is obtained. The micro-crawler ARRIpede discussed in [9] by Murthy et. al., was manufactured with the stick and slip motion characteristics actuated with the external power supply. It was manufactured from multiple chevron type actuators. This ARRIpepe manufactured was with a different manufacturing process called 2 1/2 D MEMS.

The constraint on the dimensions of the micro-robot of the order of micrometers (μm) is one of the main concerns in the robot design. External factors such as dust particles, friction, coefficient of heat absorption from the laser input source, coefficient of heat dissipation rate to the external environment (in the form of conduction, convection and radiation), maneuverability, etc. are the main aspects or requirements in the design procedure. Several paper have discussed about different robotic design methods actuation with different sources. In [27], Floyd et. al., , discuss about magnetic actuated micro-robot of micro dimensions (250x130x100μm) that can maneuver on smooth surfaces upon external magnetic excitation with a forward speed of 2.8 mm/s. A similar magnetic actuated micro-robots are proposed in [33] for fluidic manipulation by Diller et. al.. A thermal actuated bimorph constructed and modeled in [19] &

[34]. The principles of “hot” and “cold” arms are discussed with special emphasis on the mode of operation and the characteristic responses i.e. force and displacement of the system with input bandwidth and dimensions (width of one arm with respect to another) has been modeled. The actuation principle for the actuation for the actuator is heat which can be available from laser source or input source voltage.

This thesis report is dedicated to system identification of the micro-robotic systems and large chevron actuators based on the displacement outputs from the system based on the laser input at different bandwidth. As discussed in [19] for thermally actuated bimorphs system where the force generated from the system is μN to mN with increase in thickness of hot and cold arms. Increasing the thickness of arms has the negative impact of decreasing the operation bandwidth of laser input.

Summarizing the above said, the main characteristics of displacement and the generated force are the main concerns in designing the robot with respect to the laser input bandwidth. Micro-robots are meant to be durable to prolonged laser exposure and at variable power and frequency levels. While the large chevron actuators are meant to possess surface gold platting for connecting leads to supply voltage inputs at variable frequencies.

2) Micro-robot fabrication:

Single crystal silicon is used to manufacture the micro-robots with dimensions of approximately 550X300x10 μm each. The technology used for manufacturing these robots is called silicon on insulator (SOI) MEMS. A single silicon wafer is used for manufacturing 1cmX1cm dyes which can contain around 100-150 micro-robots etched from a single silicon wafer in a matrix 10X10 or 15X10 matrix layout. Silicon On Insulator (SOI) wafer which consists of a stack of handle wafer (fixed 400 μm), buried oxide and device wafer. Different thickness levels can be chosen so that different wafer thicknesses can be processed. Using one photolithography on each side of the wafer different holes can be etched down till the buried

oxide so that through holes can be manufactured onto the micro-robots. Hence the beams and gap between the beams can be manufactured using this process.

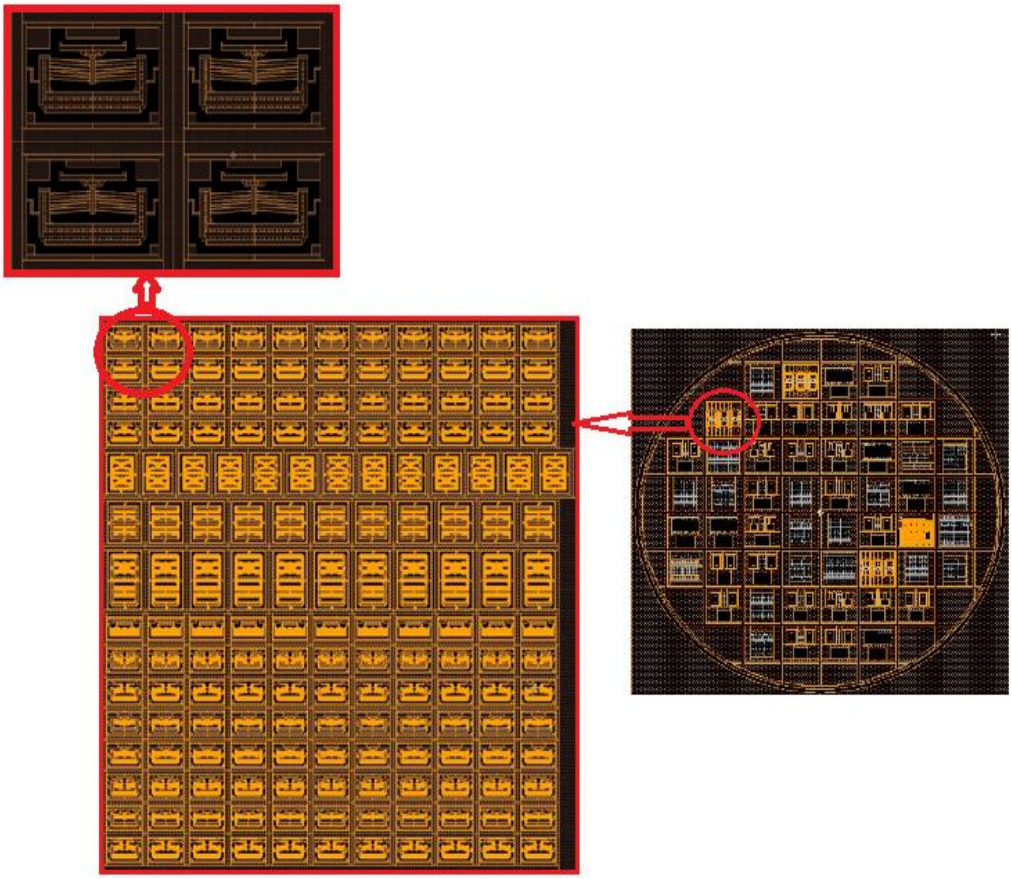

Figure 1.3 1cm x 1cm die with micro-robots

The figure below (fig. 1.4) depicts a wafer consisting of a 1cmX1cm silicon wafer consisting of micro-robots and another wafer consisting of dimples manufactured in matrix layout.

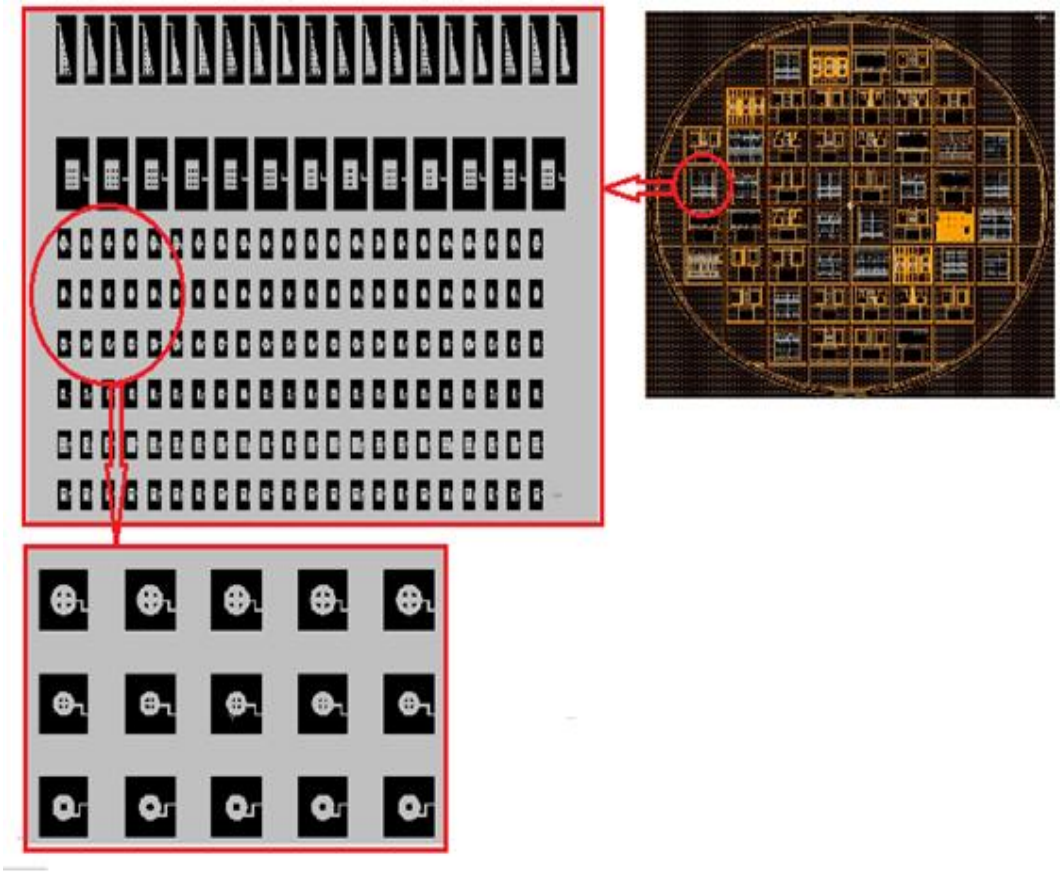

Figure 1.4 1cm x 1cm die with dimples

Dimples that will be assembled onto the micro-robot are manufactured using the same SOI fabrication process where the size of each dimple can be approximately around 65μm-200μm. Dimples of different sizes and shapes like square, circular, arbitrary shapes are fabricated. The smallest of them is around 65 μm while the largest is around 200 μm. The picture above shows a picture of dimples in matrix layout manufactured from a single 1cmX1cm silicon dye. Various processes, problems and solutions for designing the appropriate micro-assembly tools have been discussed in [7] by Popa and Stephanou where the main application scope of all the tools is for manipulating nano-scale optical cables. In [23], a vision based micro-assembly system was discussed by Lu et. al., where a sequence of micro grasping and micro joining are performed to integrate micro structures with a passive micro manipulator controlled

by a six degree of freedom robotic work station. In [13], a multi-scale robotics assembly for difference size of robots has been proposed for complex MEMS devices which act as generic framework for different types of micro or nano device manipulation and a similar approach was followed in [10]. As there is increasing need for optically actuated micro-robots, manufacturing these micro systems is a very complicated process, a special processing of micro-assembly techniques was proposed in [24] by Rabenorosoa et. al., for special class of optical micro-robots called RFS-MOB. In [25], a scalable technique for sorting sorting and manipulating micro and nano materials has been discussed by Green, Wang and Hersam which was primarily focused on sorting carbon based nano tubes based on their physical and electronic structures.

3) Test setup work for laser actuated chevron actuators:

The entire test setup is arranged on an optical desk in an isolated environment with a three degree of freedom positioning stage mounted on top of the optical desk providing motion along X, Y and rotation around Z axis, which is perpendicular to the optical desk. On top of the positioning stage, there is platform with an external supplied vacuum as shown in the below figure (fig. 1.5) labeled vacuum pump. The die containing chevron actuators sits on top of chuck, held by vacuum force. A camera is arranged on top of the die with a microscopic lens which can acquire live video of the micro-robots on the arena. Digital video output from the camera is connected to a television set and desktop computer. The desktop computer obtains images through Labview's Measurement and Automation window.

Actuation energy is provided through collimated laser beam from class IV laser source through laser head via extendable fiber is fixed at a particular angle with respect to the chuck. The laser output has a particular operating range up to few inches, hence the laser head is placed at a particular distance from the chuck so that the distance from the laser head to the chevron actuator on the arena is within that operating range.

The Laser source is of 800nm fixed wavelength source manufactured by Coherent semiconductor group called Quattro FAP-System. The system consists of single enclosure

which includes fiber array packed laser diode bars (FAP-B) mounted on top of an air cooled heat sink with all the necessary drive and control electronics. The electronics support continuous wave (CW), pulsed and external arbitrary waveform diode operation.

It has external computer interface through RS-232, with the help of Labview a standard user interface VI had been developed to control the laser sourcing and modes of operation.

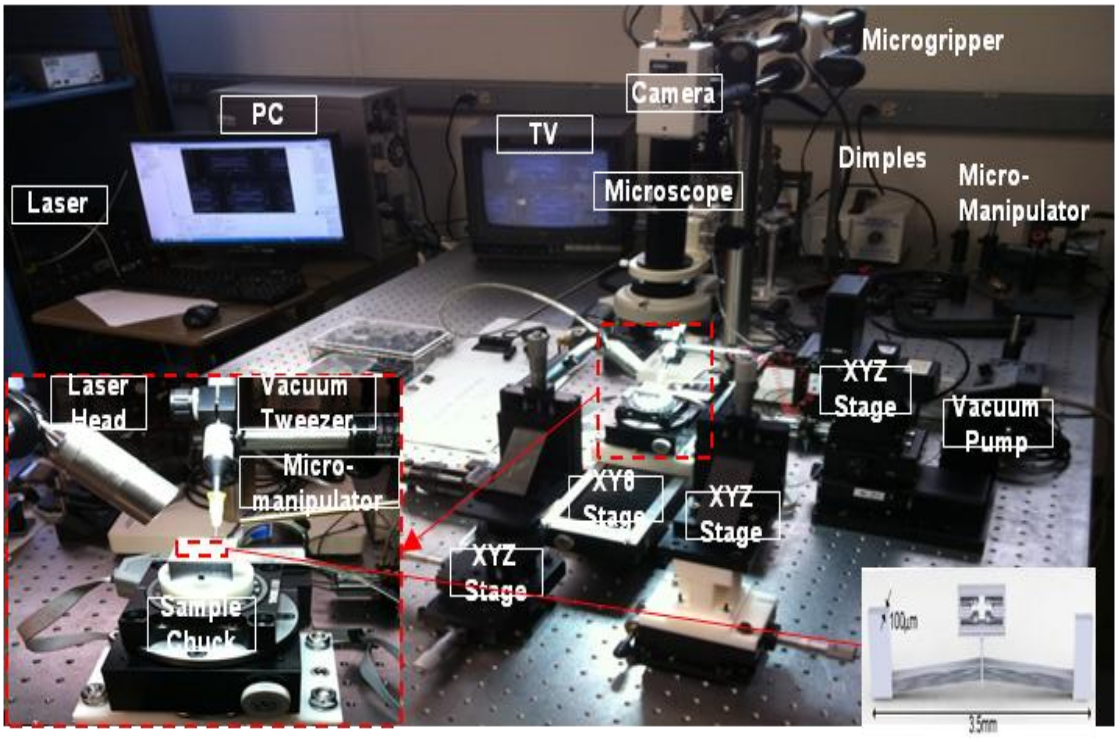

Figure 1.5 Experimental setup for laser actuated Chevrons

The iterative process of applying laser input with different combination of parameters, recording the deflections in chevron shuttle is carried out. The inputs are controlled by the software interface of hardware through Labview via RS-232 communication. The camera mounted on top of the chevron shuttle takes a precise video capture while the input laser source is applied. The camera interfaced through Labview running image acquisition software tools observes the displacement of the shuttle.

4) Test setup for electro-thermally actuated Chevrons:

The large beam chevron actuators are actuated with the help of external voltage supply. Measurement of deflection in robot with input applied voltage is carried out using interferometer techniques. An interferometer is an optical device that splits a beam of light exiting a single source into two separate beams and then recombines them. One beam called reference beam is reflected from the reference mirror, while the other beam is reflected from the surface under test. The recombined beams create an interferogram consists of bright and dark fringes representing the topography of the object. The interferogram is recorded on a CCD detector which registers the fringes and forwards them to the computer for processing using interferogram analysis software and the topography of the test surface is then generated. For obtaining measurement from smooth surfaces with very high accuracy of the order of nanometer resolution, monochromatic sources like lasers are used. One such optical bench setup with fourier Transform micro spectrometer was discussed in [14].

The above mentioned interferometer techniques are carried out on a surface profiles Veeco Wyko NT 1100-DMEMS. Fig. 1.6 shows this hardware along with voltage waveform generator. Software for using images from interferometer for constructing 3-D profile of the micro-robots is carried out with Vision (Veeco Interferometer calibration) software.

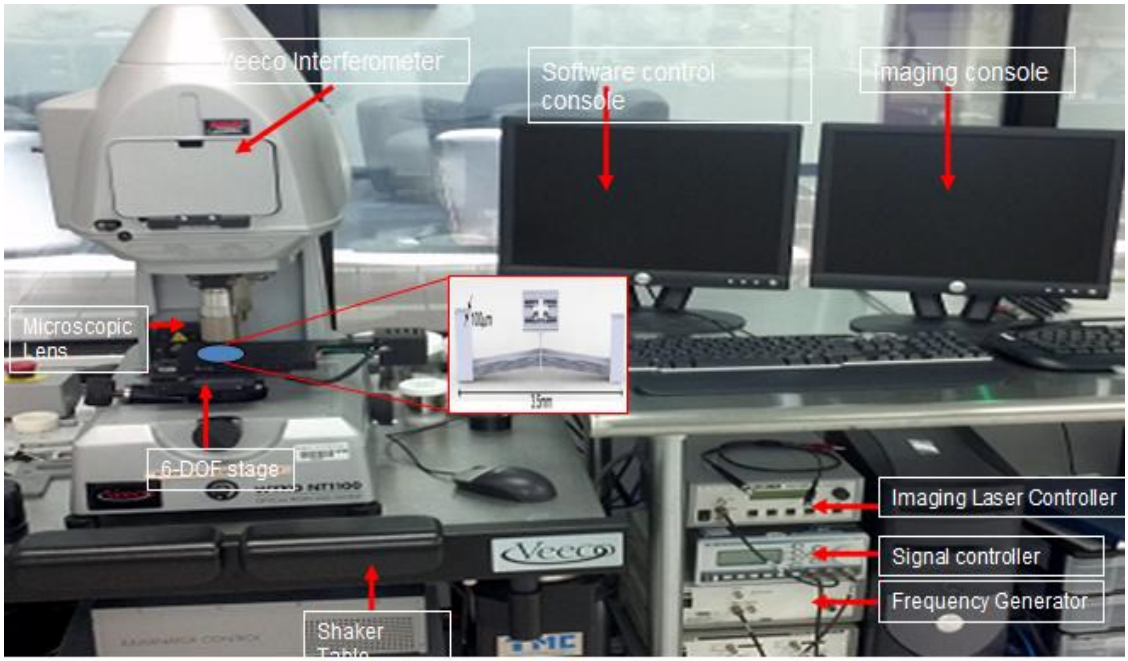

Figure 1.6 Experimental setup for electro-thermally actuated chevron actuators

For system identification of Chevron actuators, the input consists of voltage source applied at different frequencies. The Vision software has the feature to run in automation mode, where the user can select the input voltage characteristics from minimum to maximum values of frequency, amplitude, phase, type of wave (square, triangular, sine, etc.). For each combination of parameters comprising of input applied the corresponding displacement is measured and recorded. A single arm micro gripper which could measure force is arranged in such a way to measure the force measurements from the chevron actuator for the corresponding input voltage applied. The output measurement from micro-gripper simply consists of analog voltage readings, which upon normalization can be converted to force outputs. This process of interfacing, acquisition and conversion from analog voltage input from force sensor to corresponding force is carried out using Labview software.

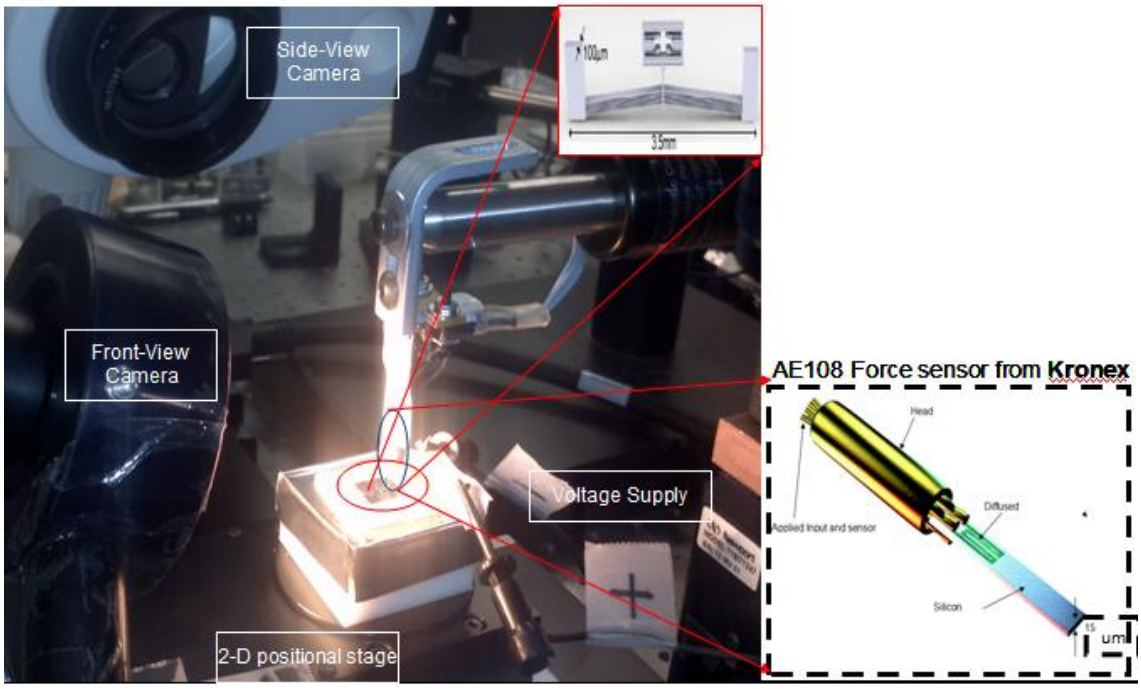

Figure 1.7 Exp. setup for force measurements from electro-thermally actuated chevrons

1.5 Contribution to this thesis

Laser actuated micro-robots and Chevron actuators are MEMS-based devices that will play an important role in the near future for applications in the field of medical, defense, biotechnology, nano electronics devices, etc. Therefore, it is important to study their dynamical behavior and create suitable dynamical models for these actuators in order to control their motion. The work described in this thesis has been concentrating on the experimental setup, acquiring i/o measurements, and performing actuator and robot system identification. For laser actuated micro-robots the single direction displacement is the main outputs with corresponding laser input characteristics (pulse frequency, duty cycle, and amplitude) are used for identification process. For current-driven chevron actuators the shuttle displacement and generated force with corresponding voltage input characteristics (wave type, pulse frequency, duty cycle, and amplitude) are used for system identification process.

The experimental work involved assembling the work station for the laser actuation of chevron actuators has been arranged for robust experiment procedure as shown in the section on the experimental test setup.

The laser source needed to be controlled programmatically for dynamic operations, where the parameters of the laser source need to be changed dynamically without laser being turned off. This process is carried out with the help of Labview. Hardware used for laser source is interfaced with RS-232 communication with the help of GUI interface using Labview.

For electro-thermally actuated chevrons, the challenges involved arranging the setup at Veeco work station. The external voltage source input hardware are available and provide at the input ports of the chevron actuator. It is controlled with the help of Vision software for changing input voltages at different frequencies. An external setup for force measurement using a single forcing sensing gripper is used with the help of Labview and interfaced to obtain necessary reading for corresponding input voltage applied.

The contributions of the thesis are as follows:

1) System analysis of micro-robots and Chevron actuators:

The laser actuated chevron actuators and micro-robots are designed at the University of Texas at Arlington by Pac and Popa. These actuators are designed with the inspiration and motivation from several other robots like “ARRIpede” discussed in [9] and thermal bimorph MEMS actuators discussed [16].The theory behind the motivation and design of laser actuator micro-actuators is clearly defined in [35].

A system-level analysis was key to the process of system identification; systems are studied to identifying the number of input and outputs with their operating range, bandwidth and the shape of input waves that can be applied to system. Based on the available thermodynamic equations an analogical model of system with other types natural occurring systems like mass spring damper, electronic circuit approximations are carried out in order to generate a lumped model for laser-actuated robots in Simulink.

2) Modeling and System Identification:

After arranging test setup as mentioned above, different inputs are applied to robot and the corresponding outputs are recorded from the device. These input, output data combinations are used in the process of system identification. A set of input-output combination, where the inputs covering the entire operating bandwidth are used for system identification process.

Based on the applied input and observed output a template model is chosen. Appropriate tuning of the parameters approximates the template model to the actual robot system characteristics. After the process of fitting a model to the data, a verification data having different input, output combination is used for verification of the fitted data model. For these set of input combinations, outputs from the identified mathematical model and robot are recorded and verified to find the convergence mathematical model to the actual physical model. If the identified mathematical model is not matching to the micro-robot characteristics, a new template model is chosen. This process continuous with different template models, with identification followed by verification. The best model that has highest approximation to physical system is chosen to be best mathematical model of the system. This model is proposed for control design of the physical systems for future applications. Recursive ARX and ARMAX models seem to be very well suited for the actuators and robots studied in this thesis.

1.6 Thesis Organization

This thesis contains the piecewise description of the entire process from theoretical foundation which encompasses the initial background study involved to the final experimental results. The background study is a source of inspiration for starting the thesis which involves understand and analyzing the properties of thermally actuated micro-robots used in the thesis, modeling and system Identification procedures used to characterize the robots from the data available. Obtaining data from micro-robots involves arranging the setup, performing automated experiments and obtaining the measurements from the microsystems. Hence the thesis has

been organized into various chapters where each chapter explains the various processes involved.

Chapter 1:

Describes the motivation on applying Modeling and identification procedure to characterize the thermally actuated micro-robots followed by the challenges involved in the designing the robots, arranging the test setup, performing experiments, modeling and identification methods to identify the system.

Chapter 2:

This chapter starts with introduction to MEMS devices followed by physical description, actuation principle, etc. thermally actuated chevrons and micro-robots. The next subsection discusses about the actuation principles, physical structure, motion mechanism of Chevron type actuators. The discussion about the equations involved displacement and force generated for a corresponding input force applied.

The subsequent subsection emphasis the thermally actuated micro-robot modeled and identified in this thesis. These robots are laser actuated with 3-DOF and have complicated experimental setup and assembly stations. Various tools have been used to manufacture these robots, to pick and place these robots for experimental setup. This further discusses about the actuation methodology, equations of motion, force generated, etc. are mentioned here.

Chapter 3:

This chapter is mainly concentrated on the experimental data graphs, modeling and identification of laser actuated Chevron type actuators. The first subsection talks about the input applied and the output obtained with graphs accordingly. The next subsection performs the system identification of the robots with software tools used, data obtained, to approximate the models to various template models. The next subsection discusses about the validations of derived models to physical chevron actuator characteristics with efficiencies and tradeoffs using

validation data. A final conclusion on the performances of different data models is discussed to derive the best model which perfectly converges to the actual physical system.

Chapter 4:

This chapter is mainly concentrated on the experimental data graphs, modeling and identification of laser actuated micro-robots. The first subsection talks about the input applied and the output obtained with graphs accordingly. The next subsection performs the System Identification of the robots with software tools used, data obtained, approximate the models to various template models. The next subsection discusses about the validations of derived models to physical laser actuator characteristics with efficiencies and tradeoffs using validation data from the micro-robots.

Chapter 5:

This chapter is mainly concentrated on the experimental data graphs, modeling and identification of electro-thermally actuated chevron actuators with displacement and force measurements. The first two sections talk about the input applied and the outputs (displacement force) obtained with graphs accordingly, with curve fitting methods approximate mathematical relationships between the input and outputs are derived.

CHAPTER 2

MEMS ACTUATORS

2.1 Introduction to MEMS Devices

Micro-robots and micro-actuators are MEMS (Micro Electro-Mechanical systems) devices with multiple degrees of freedom robots manufactured from the silicon crystal using micro or nano fabrication technology (depending on the required dimensions). These actuators can also be combined with other high conductive metals or materials to increase the conductivity of heat or current flow through the material. These systems use the basic principle of surface heating through different sources like external power supply, high power laser source, etc. for generating a corresponding calibrated deflection and inverse deflection with heat dissipation through conduction, convection and radiation. Using appropriate geometrical shaping or external assembly a pattern of stick and slip motion can be obtained to mimic the crawling behavior of biological caterpillars. These types of MEMS actuators play an important role in many applications and play dominant roles in the fields of biotechnology, inertial sensing, medical, communications, etc. where the precision and accuracy are the guidelines. Modeling and identifying the characteristics of these devices is a crucial challenge playing an important role in control design. Next two sections discuss about the MEMS devices considered in this paper for modeling and identification.

2.2 Chevron-type Actuators

These are a special class of MEMS devices where the body is manufactured with silicon with surface plating on the top with different elements. These devices use external power (voltage) supply which in turn generates heat used for actuating the device. The Chevron-Type

actuators are basically constructed with three rectangular blocks placed in parallel at equidistant to each other. Sets of pairs of beams facing each other are used for connecting these blocks at an angle called pre-bend angle. The number of beams defines the characteristic heat absorption capacity of the device. The pre-bend angle defines the specific directional motion of the device. The two external blocks on the either sides are anchored to the surface, while the central beam called shaft is suspended with the help of beams. As shown in the below figure (fig. 2.1), the beams are arranged in a geometry where the heating of beams through external power supply connected across the outer rectangular blocks causes the heating of beams. This leads to expansion of the beams producing a forward displacement of the central rectangular block called shaft or shuttle. Upon cooling the beam contract producing a reverse motion of the central shaft. The expansion of each beam is dependent on the coefficient of heat expansion of the material of the beam and the initial beam length. Since the beams are made of silicon, a linear coefficient of $3x10^{-6}$/°C.

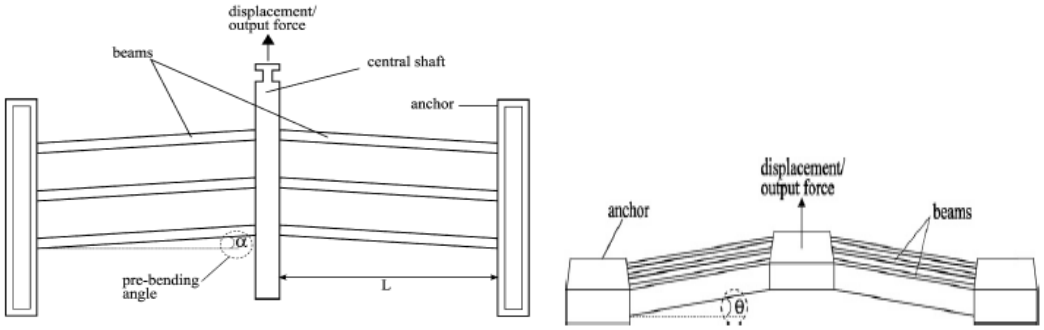

Figure 2.1 Chevron-type for horizontal and vertical motion

The operating principle of these heat sensitive beams is known as Joule heating. The voltage applied across the terminals of the anchor caused the heating of the beam due to Joule heating. According to [35], the deflection of the central shaft with ΔL change in length of the beam which is initially at L and at pre-bending angle of α is given by:

$$Def_{shaft} = (L^2 + 2L(\Delta L) + Lcos^2(\alpha))^{0.5} - L.sin(\alpha) \quad (2.1)$$

Different types of chevron actuators with different displacement characteristics can be designed. A single chevron actuator with specific deflection along both horizontal and vertical motion can be produced, the pre-bending angles α (which correspond to horizontal deflection) and θ (which define the vertical deflection) define the result deflection of the actuator. Chevron actuators have specific force generation characteristics dependent on the dimension and the rate of heat absorption due to input supplied power.

Special classes of chevron actuators which can also be powered by the laser is shown below along with dimension and have been tested.

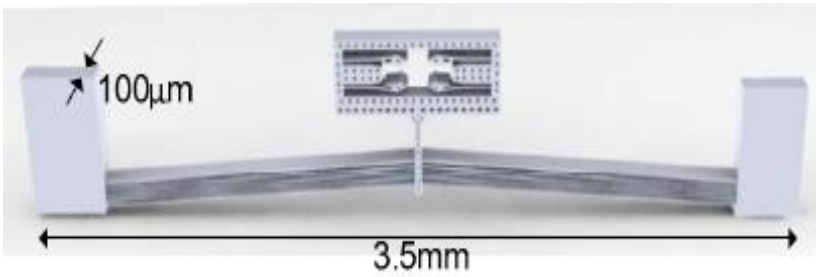

Figure 2.2 3.5mm x 100µm Chevron actuator

These are 3.5mm x 100µm range actuator which has 3.5mm beam length, with 2 anchors of 100 µm thickness. The central shuttle is in turn connected to a large rectangular block. The large beams are used for absorbing the laser source, convert to heat and transfer that heat to the beam for better heat response. The heat absorbed results in beam expansion and thus pushing the shuttle out of the body. Likewise, as the laser is turned off, the beams lose heat energy to the external environment through conduction, convection and radiation. This results in the contraction of the beam to their nominal position resulting in pulling the shuttle back into its body. Two main factors contribute to the displacement rate and force generated by the shuttle. The first factor is the volume of the beam, the more the length of the beam exposed to the heat more the expansion length of the beam result in larger displacement of the shuttle. The second factor is the number beam, more the number of beams of uniform dimension, the better the heat reception capacity from the laser source increasing the efficiency. If increasing

the beam length is constrained, the number of beams can be increased to compensate for the length constrained.

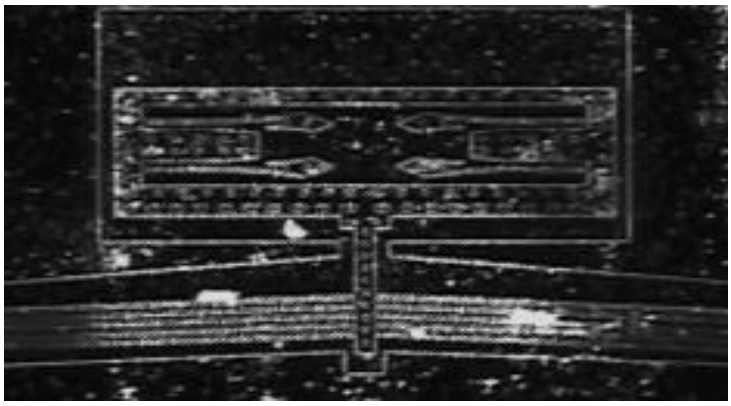

Figure 2.3 Chevron actuator where motion is induced by laser pulses.

The above figure (fig. 2.3) shows the laser actuation of the chevron actuator. A significant amount of laser radiation falls on to the surface of the additional rectangular block of the shuttle. This radiation converts to heat and is conducted to the beams. This heat in turn expands the beams. Depending on the manufacturing capability and complexity, beams can be made with different materials exhibiting different coefficient of heat expansion capability. Having able to manufacture such actuators gives additional flexibility to design micro-robots with multiple degrees of freedom. The significant property of heat expansion relating to the input applied frequency contributes to the advantage of controlling the motion of the robot with change in the input applied frequency In [36], a photo thermally actuated micro-robot is discussed with prime focus on using micro lenses to concentrate the photo energy at a specific location on the micro actuator for a desired and controlled actuation which was further continued in [37] by Baglio,et. al.. A conventional light actuated micro-pump is discussed in [42] by Mizoguchi et. alwhere an array of micro-cells are used for controlling the actuation of micro-pump based on photo-thermal energy.

2.3 3-DOF Un-tethered Micro-robot

These are some special class of micro scale robots developed by Pac and Popa in [35] based on the principle of differential thermal dynamics characteristics of the robot. As shown in the below figure (fig. 2.4), the robot has a set of beams attached to the central shaft.

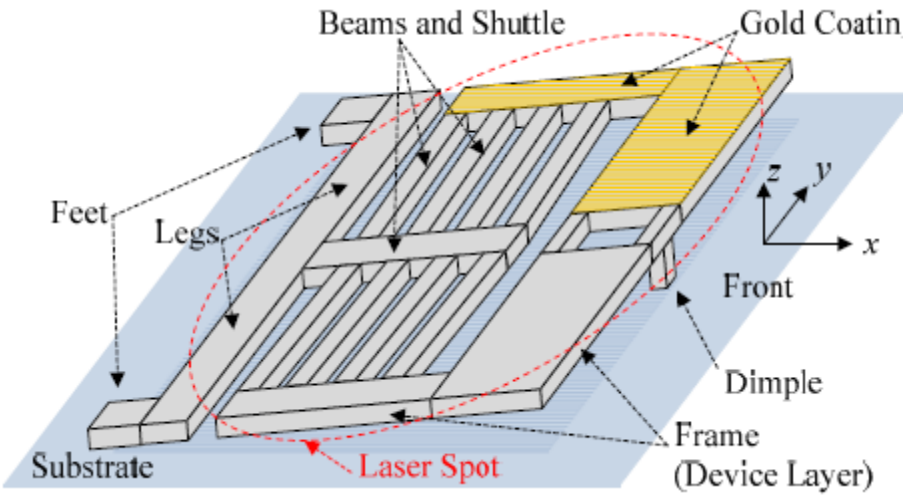

Figure 2.4 3-DOF Un-tethered micro-robot (Courtesy: M. R. Pac)

The shaft is connected to another rectangular block containing 2 legs with feet attached at the either ends. A dimple at the front maintains a fixed height avoiding contact with the surface. This dimple is placed to maintain minimal contact with the surface reducing friction and stiction due to thermal bonding with the substrate due to the heat generated from the laser, restricting the desired deflection of the robot. The large frames on the front act as the source of heat reception blocks from the laser source generating heat which in turn flows into the beams causing them to expand. The frames on the front (left and right) are thermally insulated reducing the flow of heat from one frame to another. This thermal insulation is an important characteristic of the entire architecture helping in the differential heating of the beams. The beams are directly heated from the heat supplied by the frame that they are attached i.e. the array of beams on the right half of the robot are heated from the heat supplied by the frame painted yellow in the above fig.2.4, similarly the array of beams on the left are heated by the frame in grey color. This

differential heating property is mainly governed by the variation surface material and the shape of the robot. Materials with high reflectivity have less heat absorption capacity supplying less heat to the beams which in turn affect the entire heating of the surface. As likewise, the surface area exposed to the laser source play a dominant role, the larger the surface area exposed to the laser source better the heat absorption ratio. The same applies with cooling rate of the robot. These interesting properties contribute to the differential heating and hence differential motion of the robot. Designing robots with appropriate materials which exhibit dynamic properties i.e. with respect to the applied input laser frequency, it is possible to overcome the maneuverability constraints of the robot motion.

Depending on the pre-bend angle of these beams, the shaft may either move forward which in turn pulls or pushes the feet connected by legs. The pre-bend angle of the beams has been arranged in such a way that the feet are pulled instead of being pushed. Since the geometry of the feet is such that they stick in one direction when pushed away from the body, slip when pulled toward the body of the robot. Similarly, the front dimple sticks to the surface while the rear feet slip into the body. This means that the dimple and rear feet are at negative phase with each other. As the heat absorbed by the beams dissipate either through conduction, convection and radiation, the beams start reverting back to their original initial position. At this stage, the rear wheel stick to the substrate due to the pushing action of the shuttle away from the body while the front dimple exhibit the behavior of slip result in forward motion of the entire body of the robot. The below figure (fig. 2.5) shows the side view of the robot during the stick and slip motion of the entire robot during expansion and contraction.

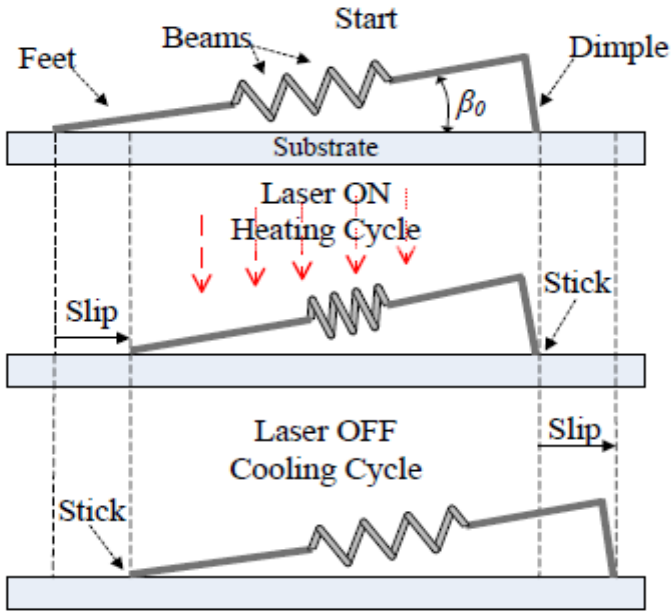

Figure 2.5 Side view of stick and slip motion of the robot (Courtesy: M. R. Pac)

The number of beams N defines the deflection rate of the entire system. The differential thermal characteristic of the robot is governed by non uniform coating of the surface with other high reflective materials which possess variation reflective characteristics with frequency of the applied laser input source. In the above fig.2.4, the left front frame of the robot is coated with gold platting, which exhibits the same heat absorption properties as silicon for certain frequencies, but has high reflective rates comparative to silicon at other frequencies.

Hence, due to this differential heating property of the entire robot surface due to the material property of the surface different motion profiles can be obtained with the input laser frequency variation. At certain low frequencies where the reflective rate of the gold surface is almost close to that silicon, the robot exhibits a forward motion. This is due to the uniform heat distribution into the beams from the left and right frames which in turn leads to equal heating of the beams.

While applying the laser input at different band of frequencies, the robot exhibits a rotational motion as shown in fig. 2.6.

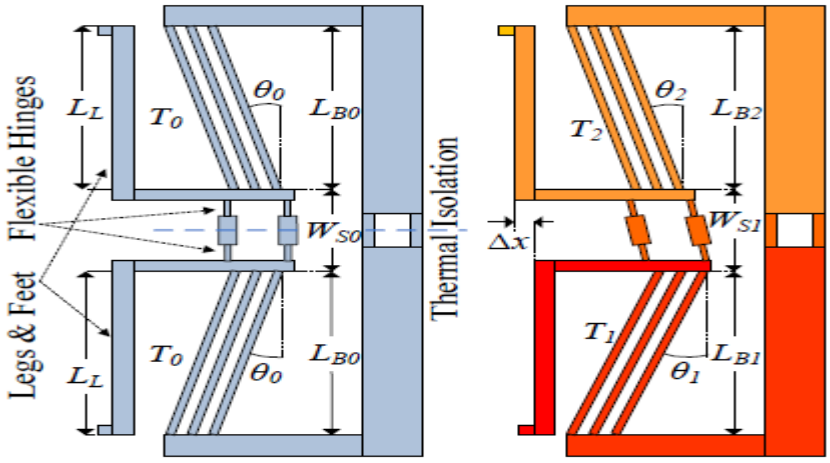

Figure 2.6 Top view of stick and slip motion of the robot (Courtesy: M. R. Pac)

From the above figure (fig. 2.6), the robot (left) in the diagram in blue color is a scenario due to the uniform heat distribution of entire surface from the heat generated by laser source at certain band of frequencies where entire surface materials exhibit equivalent heat absorption response with respect to the input laser frequency applied. This results in a uniform forward motion of the entire robot surface in the forward direction. The beams are at uniform temperature of T_0 and the pre-bending angle increases to θ_0, resulting in forward motion of the entire body of the robot.

With a different band of laser input frequencies applied the robot exhibits different characteristics, due to the non-uniform heat absorption characteristics at these bands of frequencies on the surface frames. As in the above case since the frame(left) coated with gold has high reflectivity compared to frame(right) without coating, the heat absorbed by left frame is less compared to right frame. Two flexible hinges connecting the beams on the left with the beams on the right contribute to rigid less twisting of the body. These are similar to the Automobile differential system which contributes to speed variation of the rear wheels. Some interesting discussions of non-holonomic and multiple degree of freedom micro-robots are described in [11], [12] by Murthy and Popa. During the cooling phase of the robot, the entire body of the robot expands back to its original phase where both the rear foot exhibit stiction and

the front dimple slips in the forward direction. The pre-bending angle of the right beams increases to θ_1, while the left beams increase to θ_2 where $\theta_1 > \theta_2$ and the right foot is ahead of left foot by Δx, thus rotating the entire body of the robot towards left. Thus the robot has three degrees of freedom, two orthogonal axis on the plane and rotation along the vertical axis perpendicular to the surface of the robot. The inspiration for these micro-robots came from [38] by Fatikow and Rembold and [39] by Pelesko and Bernstein which introduce the necessary fundamentals for micro-systems dynamics. The equations describing the complete motion of the micro-robot are described in the next chapter.

CHAPTER 3

SYSTEM IDENTIFICATION OF LASER ACTUATED CHEVRONS

3.1 Experimental results of Laser Actuated Chevron Actuators

The large beam Chevron Actuators are thermally powered devices where the heat from any source can be used for actuation. In this chapter we describe the laser actuation of the chevron actuators and system identification of the system from some approximations.

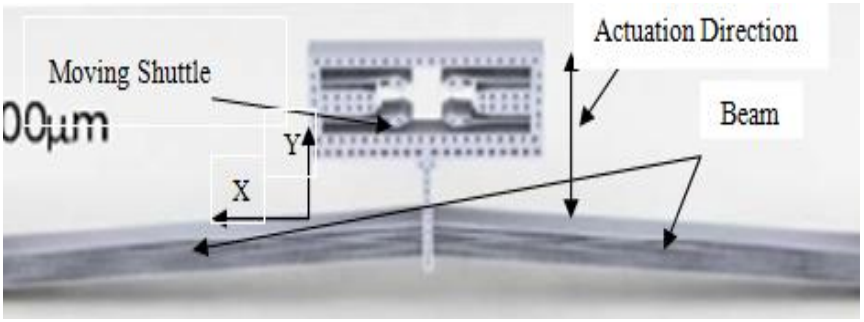

Figure 3.1 Chevron Actuator 3.5mm length and 100um thickness

Fig. 3.2 shows the methodology for conducting experiments with the laser setup and chevron actuators, as well as the process of data acquisition and system identification.

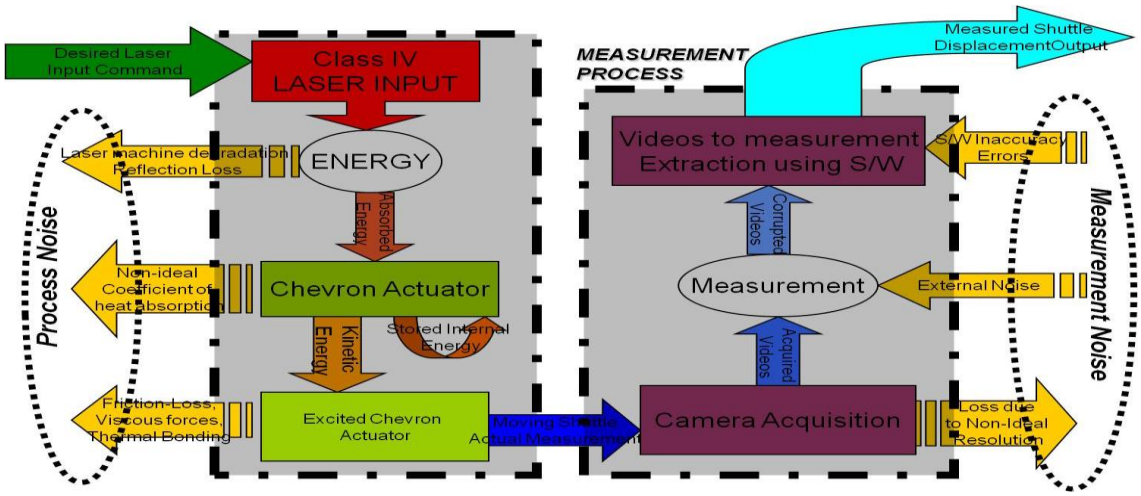

Figure 3.2 Schematic state flow of Laser actuated Chevron experiment

Experimental Results:

Laser source with different parameters have been applied to the Chevron actuators and the corresponding displacement of the center beam have been recorded with a camera. The fig. 3.3 shows the software reconstructed laser pulse marked in red. While the corresponding displacement measurements recorded through a video camera are depicted in green. Chevron actuators have single degree of freedom along Y-axis with respect to the coordinate system marked in fig.3.1. Hence the figures below (fig. 3.3-3.7) mark the displacement of the Chevron actuators shuttle along Y-axis for the corresponding input laser Pulse.

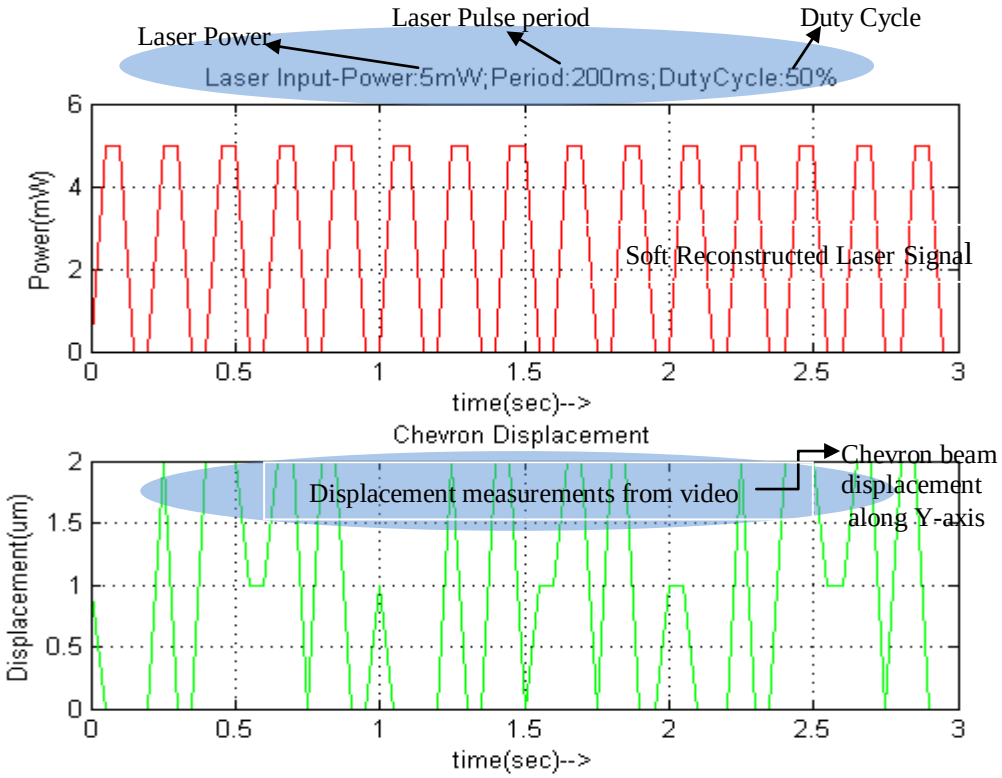

Figure 3.3 Laser pulse at 5mW-Power, 200ms Period, 50% duty cycle; Chevron beam Displacement along Y-axis in um, X-axis displacement is always measured zero.

Similarly, below figures (fig. 3.4-3.7) depict different experimental results containing laser pulse power applied and the corresponding chevron beam displacement.

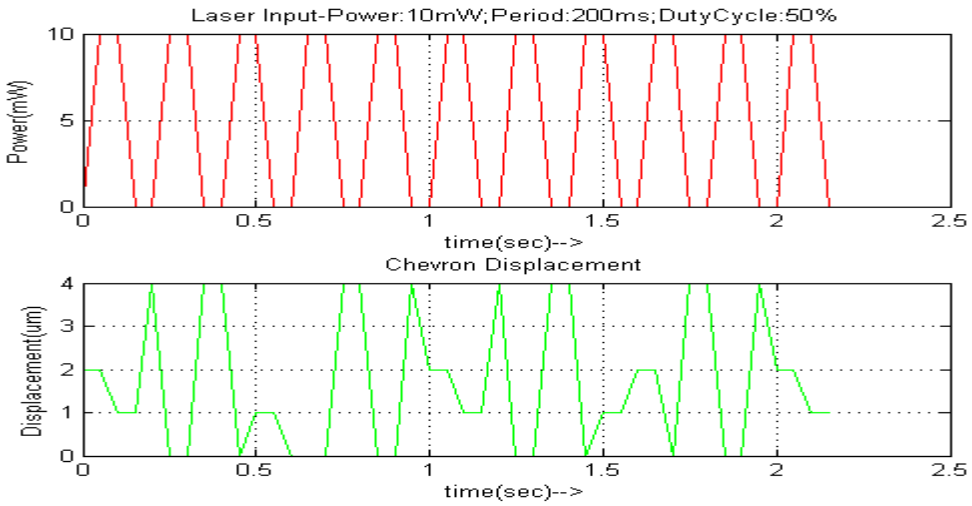

Figure 3.4 Laser pulse at 10mW-Power, 200ms Period, 50% duty cycle; Chevron beam Displacement along Y-axis in um, X-axis displacement is always measured zero.

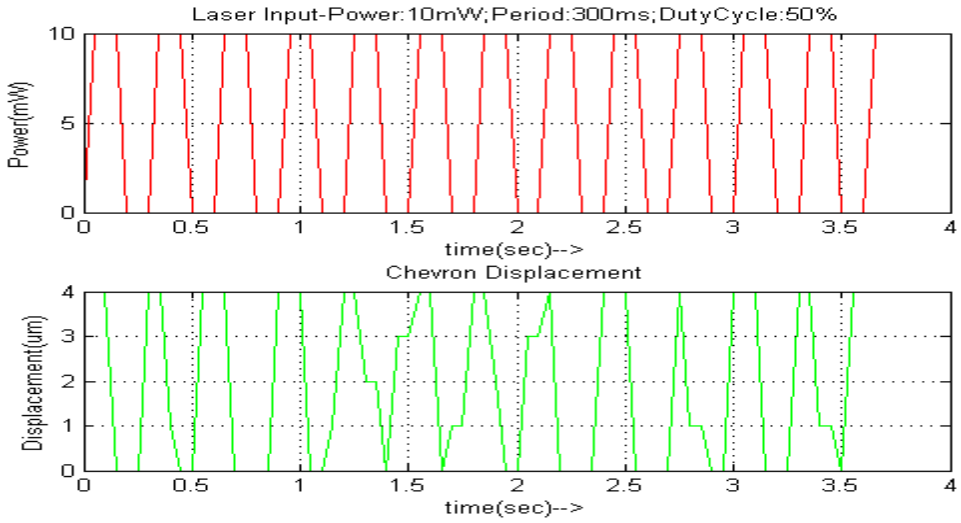

Figure 3.5 Laser pulse at 10mW-Power, 300ms Period, 50% duty cycle; Chevron beam Displacement along Y-axis in um, X-axis displacement is always measured zero

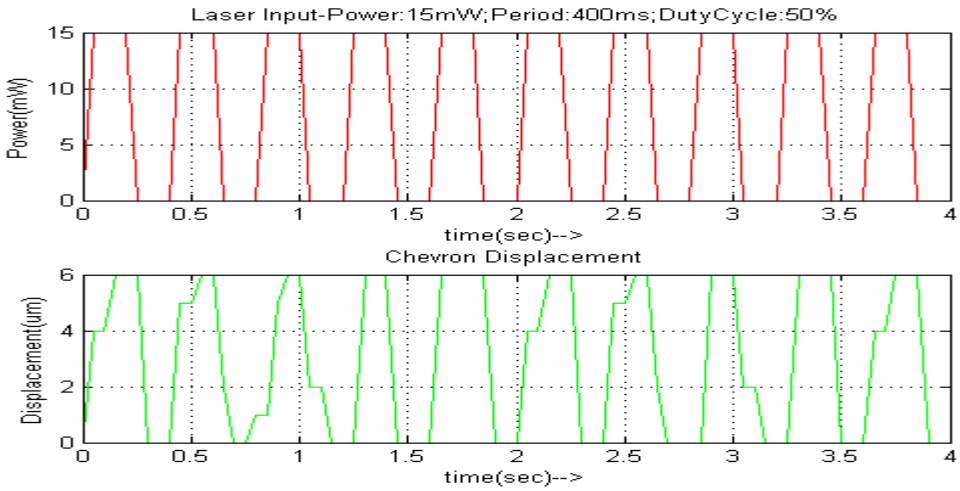

Figure 3.6 Laser pulse at 15mW-Power, 400ms Period, 50% duty cycle; chevron beam Displacement along Y-axis in um, X-axis displacement is always measured zero.

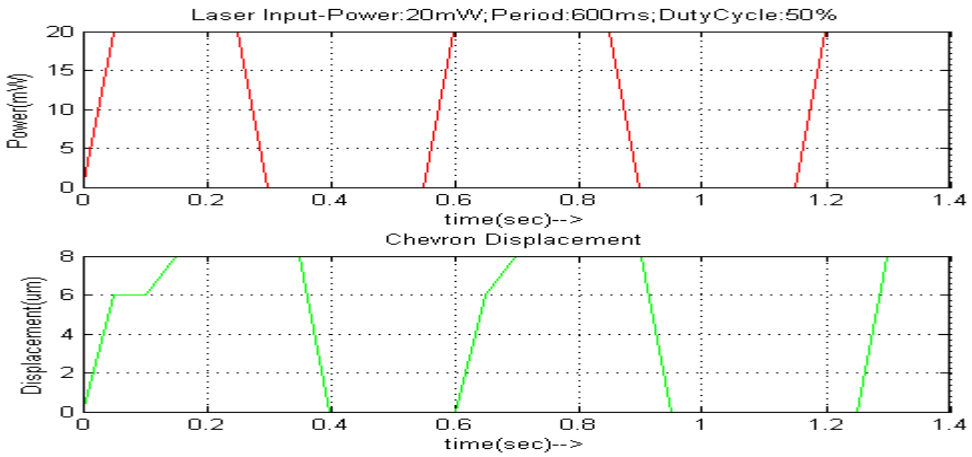

Figure 3.7 Laser pulse at 20mW-Power, 600ms Period, 50% duty cycle; chevron beam Displacement along Y-axis in um, X-axis displacement is always measured zero.

Some physical observations point out the structural damage of the chevron actuator with increasing power losing the ideal characteristic response. Hence, laser pulse with parameters corresponding up to 30mW power and 1000ms period and 50% duty cycle are used for obtaining measurements.

3.2 System identification of the Laser Powered Chevron Actuator

Upon observing the above plots several important observations can be carried out. The systems response is indirectly proportional to the applied input power and inversely proportional to frequency of the applied laser power. The system seems to behave linearly during the low frequency but behaves non-linearly in the high frequency region.

During the low frequency region, for each input laser pulse applied, the chevron actuator has the sufficient time to dissipate the heat energy before the application of successive laser input pulse. This rate of accumulation and dissipation of energy in the form of heat has a predominant impact on determining the response of the system. It depends of the properties of the material used in designing these chevron actuators. Materials with high rate of heat absorption coefficient tend to absorb heat at very fast rate. As the rate of heat absorption and dissipation increases, the system's linear behaving bandwidth increases. Both, the rate of absorption and dissipation should be high enough to contribute to the linear behavior of the system. Even though the system may seem to behave linearly in a certain bandwidth, there are many other factors that contribute to the non-linear behavior of the system.

For high frequency laser input pulses where the frequency is beyond the linear bandwidth region of the chevron actuators, the system behaves non-linear. The non-linearity is mainly contributed by the accumulation of internal storage of energy in the form of heat which produces a nonlinear behavior.

Disturbance from the external environment in the form of laser reflection, radiation, change in material properties over time, etc. are the contributing factors which affect the behavior of the system making it highly nonlinear. The data from the measurements are thoroughly effected by the measurement noise from the camera. In addition to this, the algorithms used for finding displacement measurement from the camera video recording also degrade the quality of the measurement. This measurement noise plays an important role in

reducing the linear bandwidth of the system. Hence system identification should mainly address these typical error terms in a dynamical approach for system identification.

System identification using linear methods like state space, transfer function, etc are not an appropriate choice for identification. These functions do not address the error properties from a more robust and dynamical point. In this thesis, we use some advanced techniques like ARX and ARMAX models from a static point of view as these models address errors with a separate transfer functions. These types of models are ideal in system identification if the error models have known probability distributions. In [26], Dang et. al., discuss on using the neural network concepts for optimal placement of micro-actuators where they propose extended orthogonal least squares method to estimate the position of the actuator.

Systems with unknown error characteristics need a more robust approach in predicting the future behavior of the system. A recursive approach which improves its prediction accuracy based on the past inputs and outputs are an appropriate choice. In this thesis we will be using a Kalman filter which contributes to the prediction quality. Both ARX and ARMAX models will be assisted with the recursive Kalman filter for quality improvement. The analysis of their prediction results will clearly depict their performance for static approaches.

The main aim of this thesis is to provide a launch pad for developing future control systems applications for micro-robots. A good prediction model plays an important role in improving the convergence rate of the system with optimization. The following subsections discuss about the system identification techniques used with their performances. The inspiration for the system identification of these micro-actuators comes from many papers as in [2] by Lyshevski and Lyshevski, where they discuss about three-dimensional geometry dynamics in time domain with data intensive modeling and simulation are performed on MEMS devices for micro and nano scale devices. A high-fidelity 3-D modeling is performed from the measured data to fit appropriate mathematical system models.

3.2.1 Estimation, Validation data set and Re-sampling

In this subsection, we will be discussing about the estimation and validation data used for system identification and verification. A pseudo random data plays an important role in system identification covering the entire bandwidth or the operating region of the Chevron actuators. Performing experiments on the chevron actuators using Laser source with a continuous pseudo random inputs is a very difficult task. Hence, in this chapter we will be using stitched data from multiple experiments to form a single continuous pseudo random data to be used for system identification. The figure below (fig. 3.8) shows the estimation data taking data from six randomly conducted experiments.

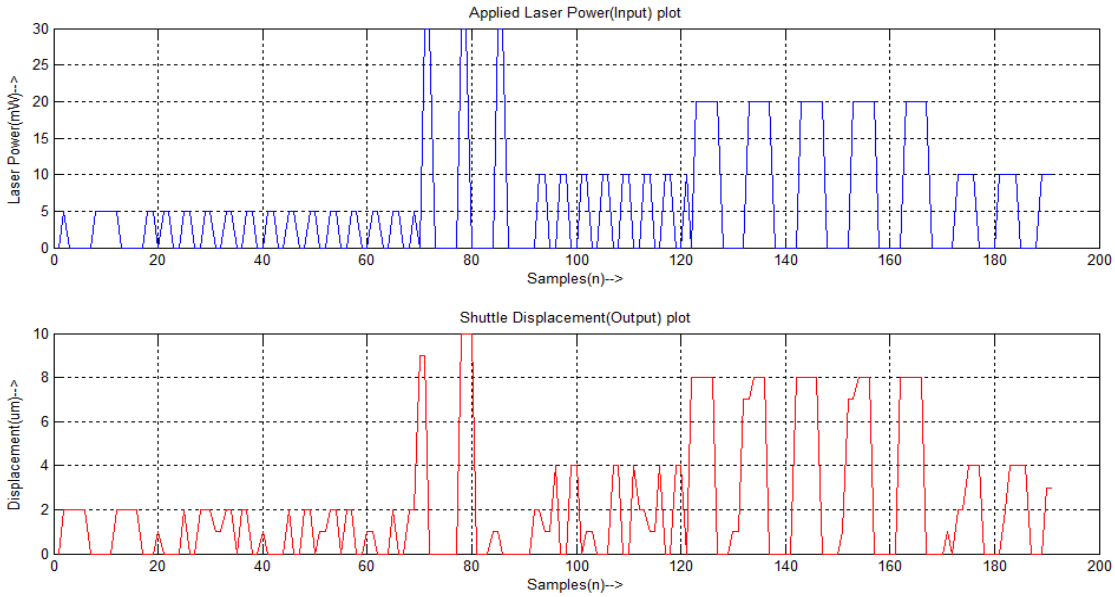

Figure 3.8 Estimation Data from six random experiments.

Re-sampling Data using curve fitting:

As can be observed in the above figure (fig. 3.8), the number of data points considered for the estimation is around 191 due to some limitations and these data points are insufficient for system identification. The response data at high frequency components may be missing due to the slow capture rate of the video camera. Hence using this exact data for identification will be wrong choice for system identification. Re-sampling the data at a higher rate from the

existing data points is a proper choice while still preserving the low frequency components. The process of re-sampling works by the principle of decimation and interpolating points between the existing data points. For generating more decimation points between the existing data points, we use interpolation techniques for fitting extra data points between the existing set of data points.

Using techniques like piecewise interpolants, a better approximation of the estimation data can be produced. The estimation data is broken into multiple segments (or sets) and a curve fitting is performed on each data segment. This type of decimation to produce more data samples has proved to be a very efficient method. The accuracy of fixing the interpolants is measured by the correlation measurement. We use MATLAB Curve fitting toolbox to produce interpolants. The figure below (fig. 3.9) shows the decimated data samples using the interpolants where we generate 1910 data samples for system identification techniques.

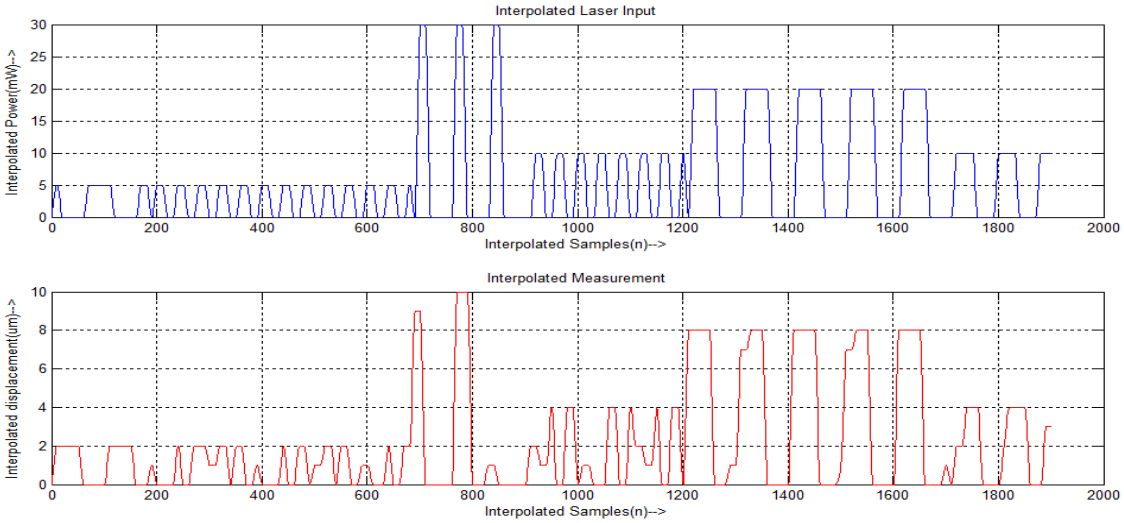

Figure 3.9 Re-sampled measurement data using interpolants

Similarly, we use validation data for validating the performance or convergence of the estimation model to the actual physical model. We may use the same interpolants to decimate the validation data to generate more data points. The Validation data will be shown in the subsequent section.

3.2.2 ARX Modeling

In this section we will be discussing on system identification using standard regression models given the below equation. In this subsection we will be discussing on the aspects of system identification using the ARX models which are build on extension to the state space model discussed in the previously. In fact, the estimated state space model is used for initializing the ARX model.

$$A(q)y(t) = B(q)u(t - nk) + e(t) \quad (3.1)$$

Where q is the delay operator.

$$A(q) = 1 + a_1 q^{-1} + a_2 q^{-2} + \ldots\ldots\ldots\ldots + a_{n_a} q^{-n_a}$$

$$B(q) = b_1 + b_2 q^{-1} + b_3 q^{-2} + \ldots\ldots\ldots\ldots + b_{n_b} q^{-n_b}$$

In this section we perform the system identification of the re-sampled data considered fig. 3.9, Using Matlab System Identification toolbox, we obtain the following values for the coefficients.

$$A(q) = 1 + 0.8182q^{-1} \quad (3.2)$$

$$B(q) = 0.3736 + 0.3355q^{-1}$$

ARX models are similar in structure to the OE model discussed in the previously, except they have better noise control characteristics with the $A(q)$ involved.

The continuous form of the ARX model is given by,

$$y(t) = [B(s)/F(s)]u(t) + [C(s)/D(s)]e(t) \quad (3.3)$$

Converting discrete ARX model in eq. 3.1 into continuous form as shown above, we obtain

$$B(s) = 0.2096\,s + 1560 \quad ; C(s) = s + 400 \quad (3.4)$$

$$D(s) = s + 4000\,;\ F(s) = s + 4000$$

From the identified ARX model it is essential to analyze the Step response of the continuous ARX Model in order to understand the system response.

The figure below (fig. 3.10) shows the step response of the system,

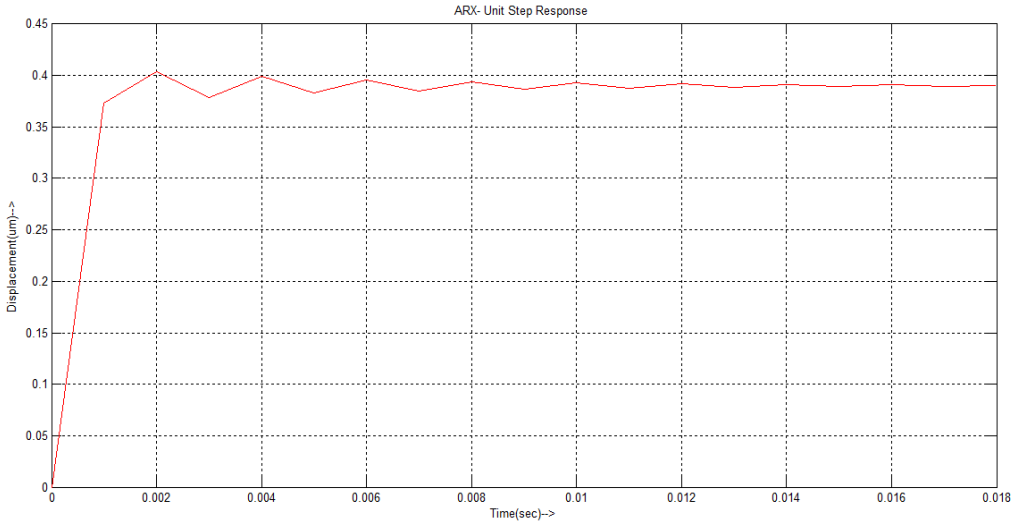

Figure 3.10 Unit step response of the ARX discrete model

The step response of the system is close to the ideal expected characteristics of the system. In the above plot the rise time and the settling time are close to the expected profile.

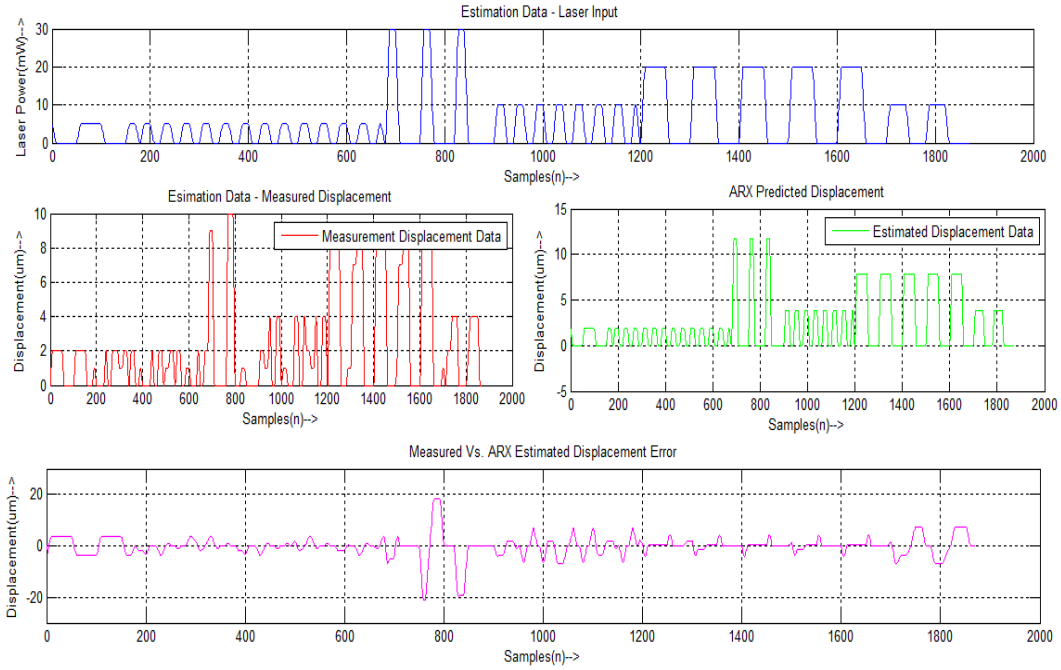

Figure 3.11 ARX with Estimation data

The figure above (fig. 3.11) shows the Estimation data input (colored blue), measurement data (colored red) and the predicted data (colored green) from the ARX model. The subplot at the end shows the prediction error (color magenta) which is the difference between the measured displacement data and the ARX model predicted displacement data for the same laser input. At around sample number 800 there seems to be high Displacement error which is purely due to the corrupted measurement. The corrupted measurement may be due to the camera video capturing error or the inconsistency in video to measurement conversion algorithm which could not read the video data properly.

Model Validation:

Validation of the obtained ARX model is carried out using the validation data as shown in the figure below (fig. 3.12). The validation data is also a pseudo random which could be used in checking the validity of the predicted ARX model. The same validation data will be used in the subsequent estimation models as it is easier to check the performance of the models.

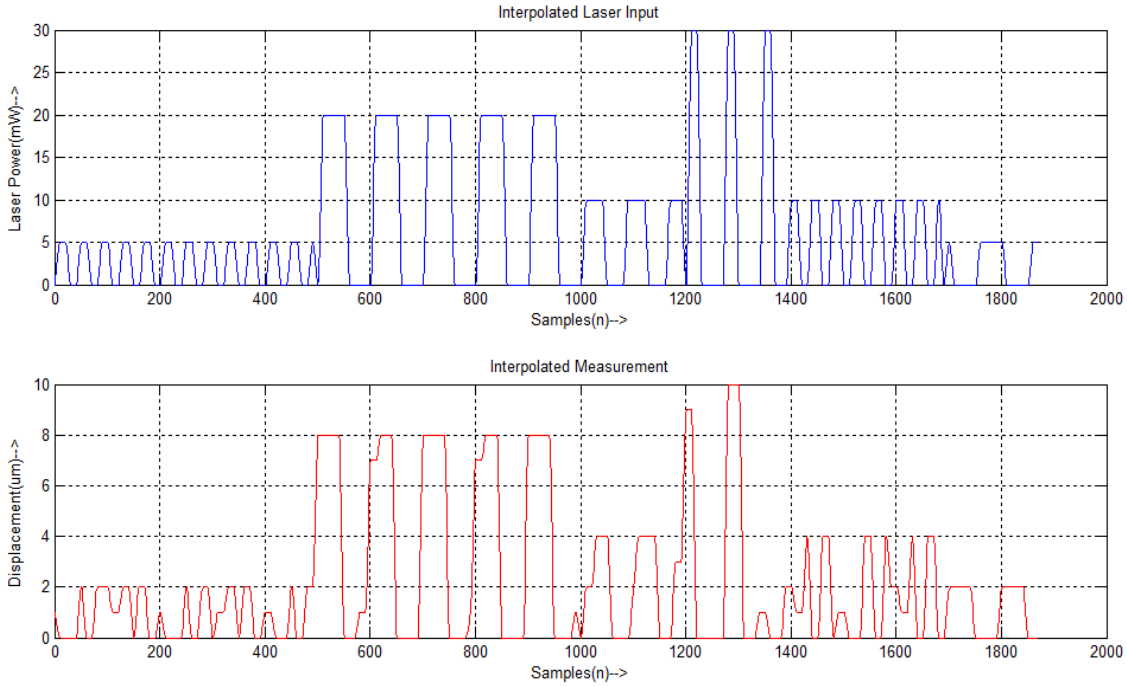

Figure 3.12 Validation Output, Simulated Model Output with corresponding Laser Input

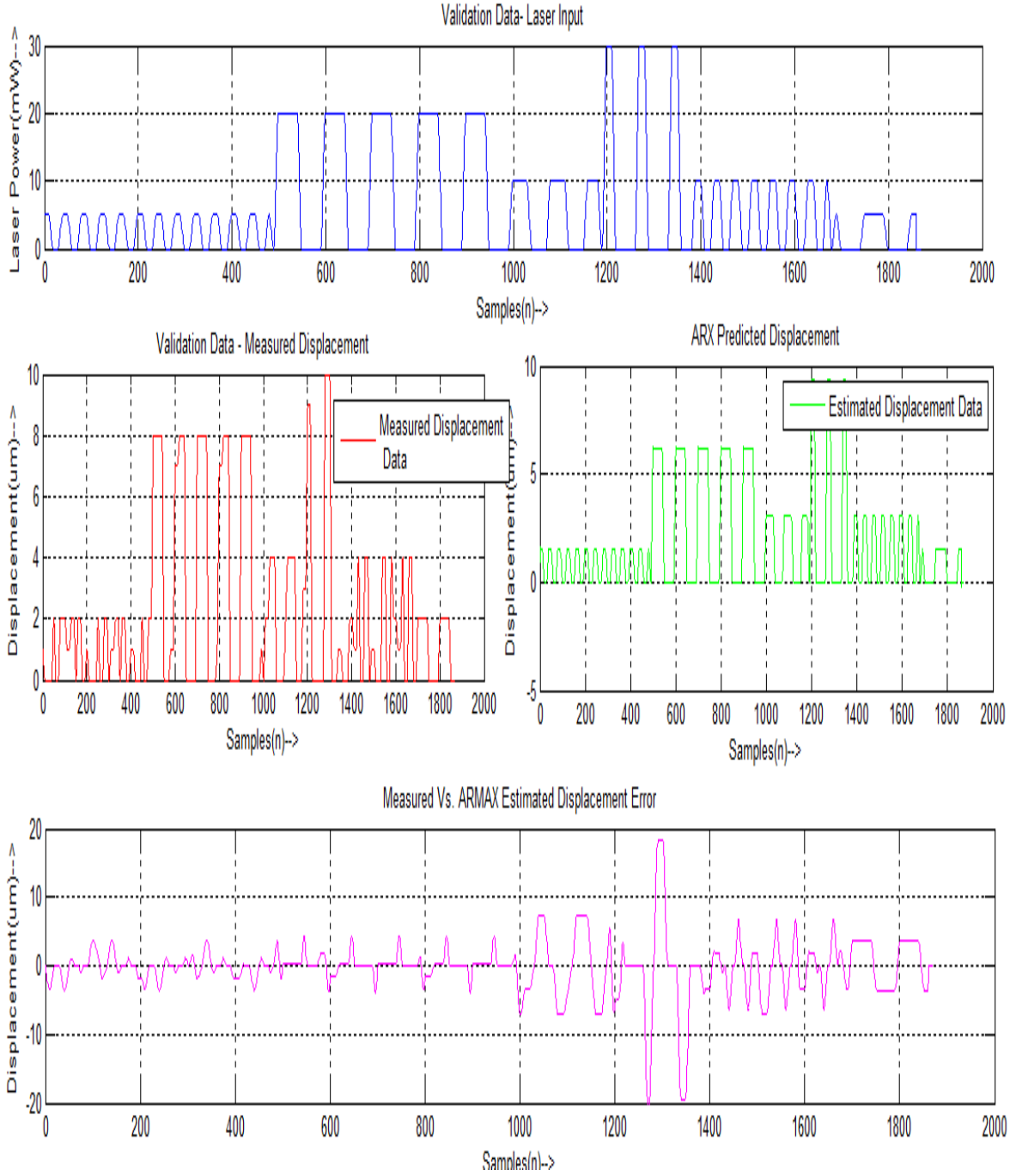

Figure 3.13 ARX with Validation data

The figure above (fig. 3.13) shows the application of ARX model applied to validation data. The color conventions are the same for all the data as explained before for estimation

data. Upon visual inspection it can be observed that the displacement error seems to suffer the same scenario as explained for the estimation data. Hence using the model performance measures to verify the convergence of the ARX model to the actual physical system is still a open question with high uncertainty. Even the estimated coefficient values may not be the accurate consistent values and may change with different estimation data. This type of uncertainty can be handled with advanced recursive techniques which perform better parameter tuning with each iteration from the previous prediction and measurement knowledge. This will be clearly shown in the subsequent subsections.

3.2.3 ARMAX Modeling of the System

In this section we will be discussing on system identification using auto regressive moving average mode (ARMAX) models given by the below equation. These ARMAX models which are build on extension to the ARX model discussed previously. In fact, the estimated ARX model is used for initializing the ARMAX model.

$$A(q)y(t) = B(q)u(t - nk) + c(q)e(t) \quad 3.5$$

Where q is the delay operator.

$$A(q) = 1 + a_1 q^{-1} + a_2 q^{-2} + \ldots\ldots\ldots\ldots + a_{n_a} q^{-n_a} \quad 3.6$$

$$B(q) = b_1 + b_2 q^{-1} + b_3 q^{-2} + \ldots\ldots\ldots\ldots + b_{n_b} q^{-n_b}$$

$$C(q) = 1 + c_1 q^{-1} + c_2 q^{-2} + \ldots\ldots\ldots\ldots + c_{n_c} q^{-n_c}$$

In this section we perform the system identification of the re-sampled data considered in fig. 3.9. Since ARMAX model are extensions to ARX models, using the coefficients derived for ARX model to initialize the ARMAX model is the appropriate choice for better approximation from eq. 3.2 to initialize the coefficients in eq. 3.6, hence we obtain

$$A(q) = 1 + 0.8182q^{-1} \quad 3.7$$

$$B(q) = 0.3736 + 0.3355q^{-1}$$

C(q)=Unknown

ARMAX models are similar in structure to the ARX model discussed in the previously, except they have better noise modeling characteristics with C(q) and $A(q)$ involved. Use the a non-linear least squares method like PEM(Prediction Error Minimization) technique discussed by Ljung in [29] to find the coefficients of new optimized ARMAX model we obtain.

$$A(q) = 1 + 0.1824q^{-1} \tag{3.8}$$

$$B(q) = 0.3448 + 0.02303q^{-1}$$

$$C(q) = 1 + 1.881\,q^{-1} + 0.28\,q^{-2} - 1.712\,q^{-3} - 1.269q^{-4} - 0.1583q^{-5}$$

Noise Variance = 73.8128

In this model the order of A(q), B(q) are with fixed order, one as specified for ARX model, while the order of C(q) has been to chosen as 5 to compensate for the high frequency noise characteristics. The effect of these noise can be observed in validation output of the ARX model where we did not have the control over noise. Finding the continuous time model (using Tustin's method) of the discrete ARMAX in eq.3.5 with the terms obtained in eq. 3.9, we obtain:

$$y(t) = [B(s)/F(s)]u(t) + [C(s)/D(s)]e(t)$$

Where,

$$B(s) = 0.3111s + 108.8 \tag{3.9}$$

$$C(s) = s^5 + 1.313e009s^4 + 7.243\text{e}011s^3 + 2.788\text{e}015s^2 + 1.537\text{e}018s^1 + 7.546\text{e}017$$

$$D(s) = s^5 + 1877s^4 + 1.403\text{e}006s^3 + 1.403\text{e}006s^2 + 9.641\text{e}010s^1 + 7.081\text{e}012$$

$$F(s) = s + 276.6$$

As can be observed, increasing order of the noise factor C(q) produces a considerable impact, thus an attempt in increasing in the order C(q) may perform better results but it could increase the complexity of the system for application to control system design. ARMAX have the advantage of producing better noise response characteristics which was quiet difficult to manage for ARX models.

The step response of the system ARMAX model shown when compared to Fig. 3.14 has a lot of important observations that we pointed out. It has better rise time with sharp

overshoot which was part of the observation during the experiments. Zero oscillations as t→∞ is a typical characteristic which is not observed in the real experiments. The chevron shuttle did exhibit oscillations which were clearly shown by the step response of the ARX model.

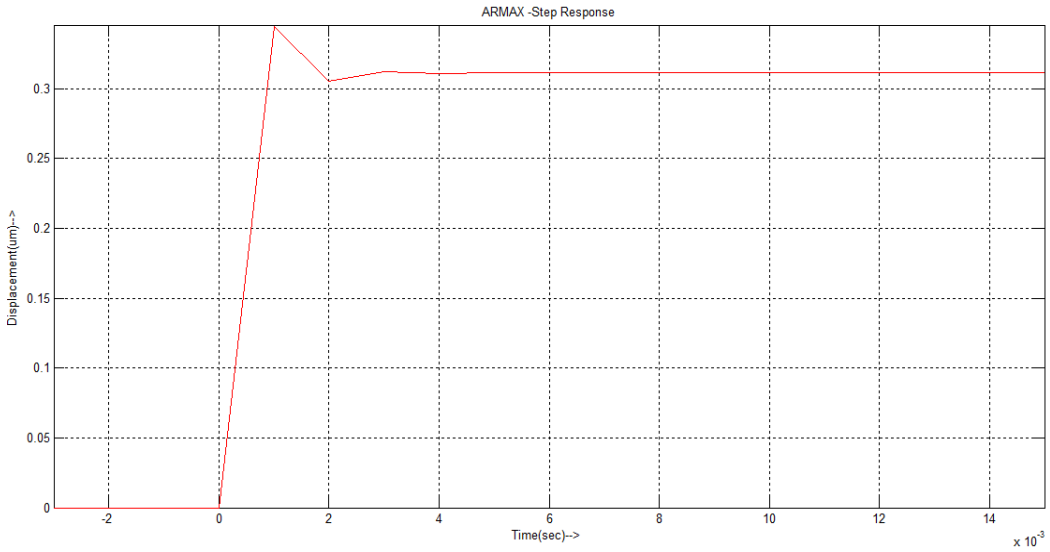

Figure 3.14 ARMAX Unit Step response of the system

The figure below (fig. 3.15) shows the ARMAX model applied with the estimation data Input. We use the same color conventions to denote the different aspects of the data plots. By visual inspections it can be observed that the ARMAX estimated output data has better response characteristics and seem to closely mimic the Input Laser. An important observation is the typical prediction error show in the last subplot (in magenta) where the error keeps increasing. This type of behavior is attributed to the phase difference characteristics induced by the ARMAX error coefficient transfer function.

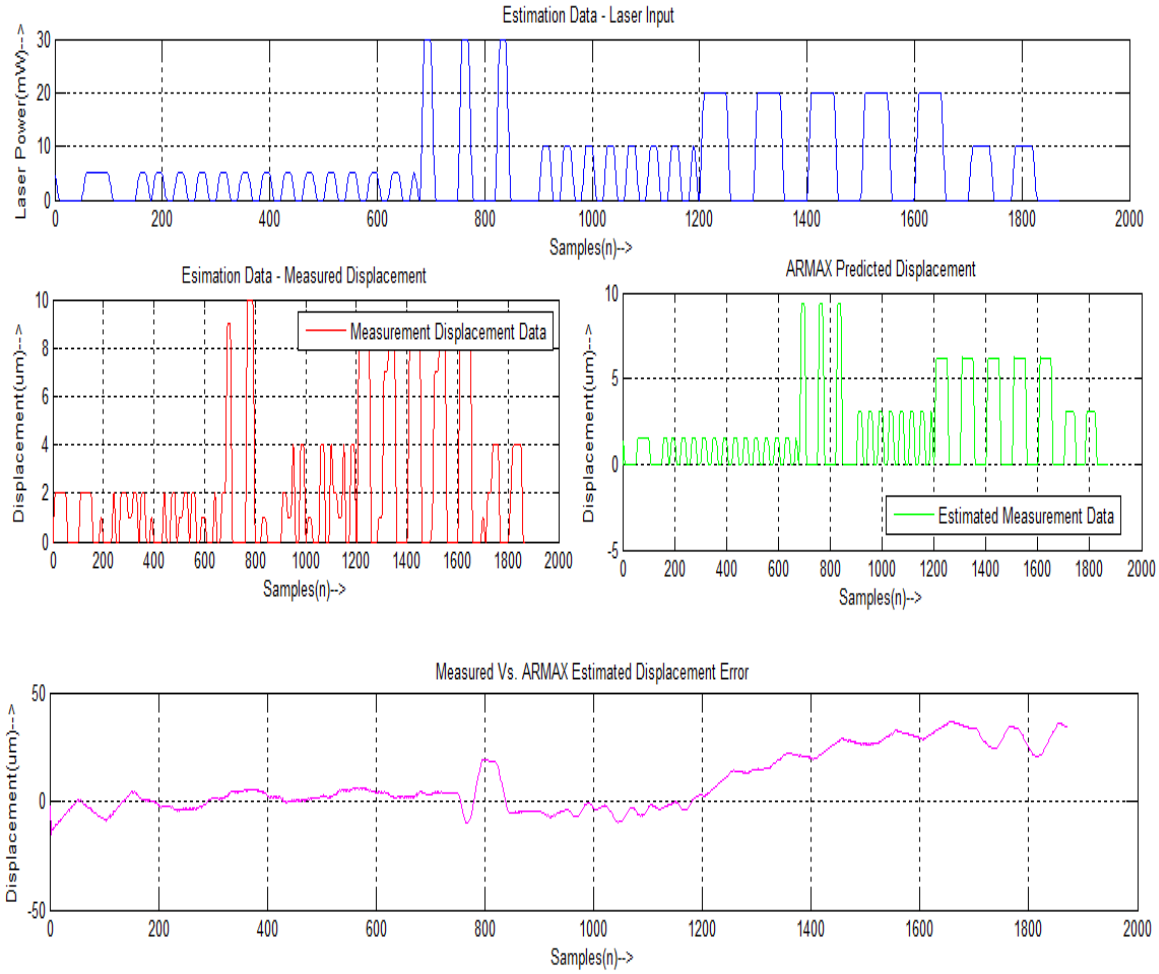

Figure 3.15 ARMAX Estimation data

Model Validation:

Validation results of the identified ARMAX model is given in fig. 3.16,

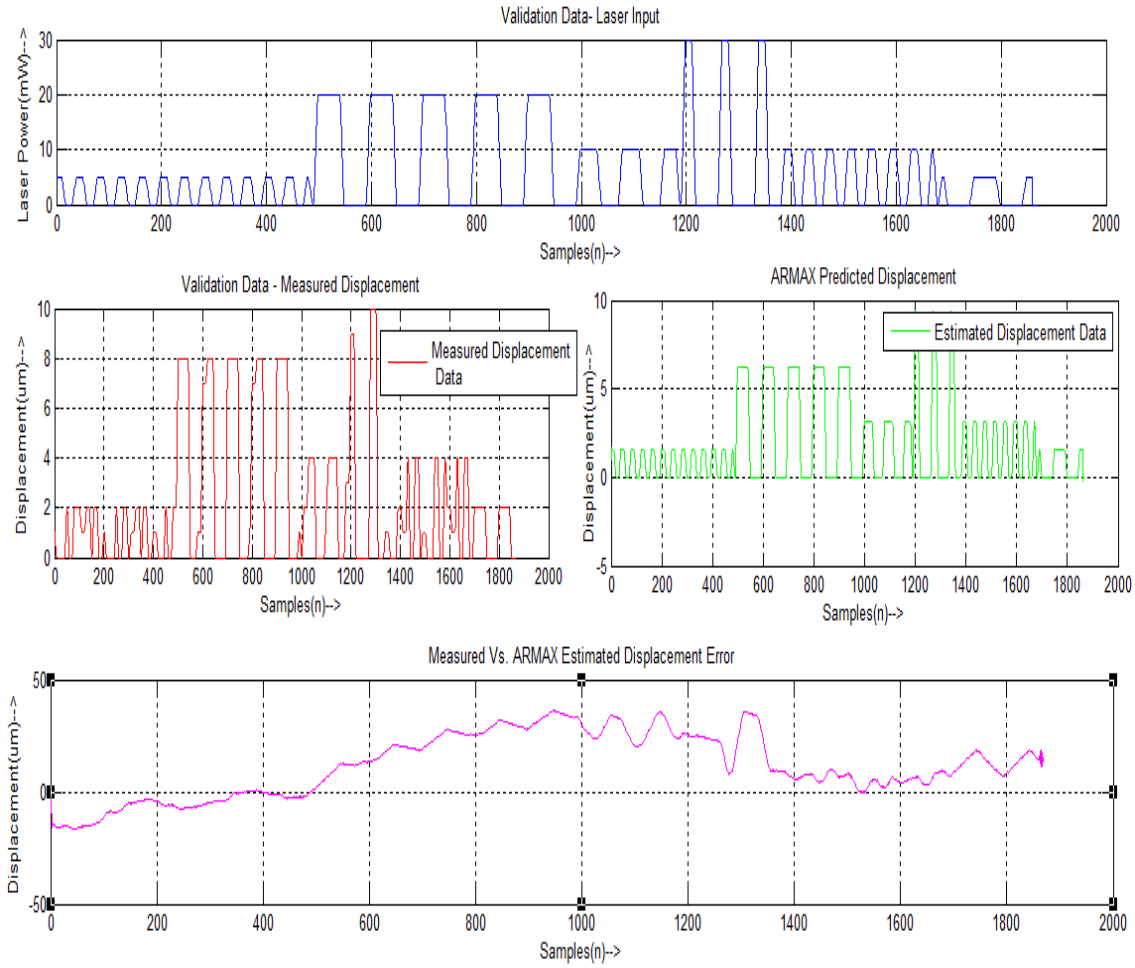

Figure 3.16 ARMAX with Validation data

From the above figure (fig. 3.16), it can be observed that the ARMAX has better response compared to the ARX model due to the noise compensation transfer function *C(q)* which improves the noise response of the system. The predictive characteristics of the system have a predominant impact of improving the fast response of the system, thus reaching the ideal characteristics of the system compensating the disturbance. These disturbances are usually in the form of friction under the Chevron or irregular heat transfer to the external environment.

3.3 Recursive Identification using Kalman Filtering

In this section we discuss about the recursive method of computing online models fro better prediction. Different Algorithms used for recursive parameter estimation are employed in various papers. The common and the most efficient method of online parameter(s) calculation used in this section is based on Kalman filter algorithm also known as Recursive Least Squares (RLS) method. In this section we will be discussing about using Kalman filter algorithm applied to ARX, ARMAX models. The flow diagram given below gives a description of the online parameter identification using a Generic Kalman Filter.

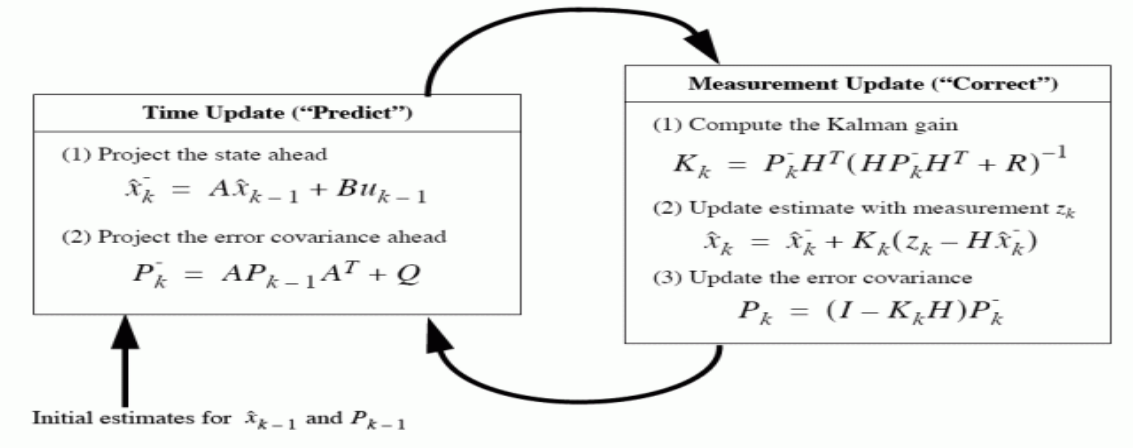

Figure 3.17 Generic Kalman Filter Algorithm flow for parameter Identification (Wiki)

The detailed description of Kalman filtering algorithm for online parameter calculation is specified in [29], only the application results of Kalman filtering to ARX and ARMAX are discussed. The flow diagram in fig.3.17 is source of reference for all the recursive algorithms discussed in the rest of this thesis. Inputs to recursive algorithms are the initial state values, initial covariance matrix of the unknown parameters in the model, corresponding order of the systems, initial parameter values. Initial covariance matrix should be a square matrix equal to the number of unknown parameters. Initially defined order of the system defines the unknown parameters in the system. The performance of the Kalman filter is dependent on the number of data points and initially defined parameters. Hence, convergence rate of the recursive methods

defined below for OE, ARX and ARMAX are dependent on the number of data points as well as their transfer function characteristics as defined in the previous section.

3.3.1 Recursive ARX with Kalman Filtering

Applying recursive approach for a below given ARX,

$$A(q)y(t) = B(q)u(t - nk) + e(t) \tag{3.10}$$

Where q is the delay operator.

$$A(q) = 1 + a_1 q^{-1} + a_2 q^{-2} + \ldots\ldots\ldots\ldots + a_{n_a} q^{-n_a} \tag{3.11}$$

$$B(q) = b_1 + b_2 q^{-1} + b_3 q^{-2} + \ldots\ldots\ldots\ldots + b_{n_b} q^{-n_b+1}$$

We know that the convergence rate of the system depending on the proper initialization of the unknown parameters. Hence using the parameters derived in subsection 3.2.2 in eq. 3.2 for initial parameter values. Since we have already obtained reasonable values for the unknown parameter values, it is always an added advantage to use these parameters for initialization.

Model order = $[n_a\ n_b\ n_k]$ = [1 2 0]

$$\text{Initial Parameter Covariance Matrix} = P_0 = \begin{bmatrix} 0 & 0 & 0 \\ 0 & 0 & 0 \\ 0 & 0 & 0 \end{bmatrix}$$

Initial Parameter values= $[a_1\ b_1\ b_2]$ = [0.8182 0.3736 0.3355]

We are not yet sure of the initial covariance matrix which can be set to zero. Hence, applying recursive Kalman method to the estimation data as before, we obtain the following result shown in fig. 3.18. The noise model has a predominant impact on the system which has much better approximation to the system noise. The parameter covariance matrix, predicted parameter values obtained at the end of the simulation are given below:

$$\text{Final Parameter Covariance Matrix} = P_N = \begin{bmatrix} 0.0809 & 0.0721 & -0.0527 \\ 0.0721 & 0.7454 & -0.7256 \\ -0.0527 & -0.7256 & 0.7158 \end{bmatrix} * 10^{-3}$$

Final Parameter values= $[b_1\ \ b_2\ \ f_1]$ = [-1.0196 -0.0648 0.0542]

An important observation that can be pointed out is the reduction in prediction error show in the last subplot of fig. 3.18 colored in magenta. The color convention of all the subplots in the fig. 3.18 are the described before and is clearly written.

Compared to fig.3.11 the absolute prediction error which was more than 1 has reduced to less than 1 which was a better improvement. The error at around sample number 800 is mainly due to the missing camera reading or other factor which was explained previously.

At this point the Kalman aided ARX model has the ability to simulate camera measurement error and the other unexplained noise characteristics characterized by the noise from the surroundings as explained before.

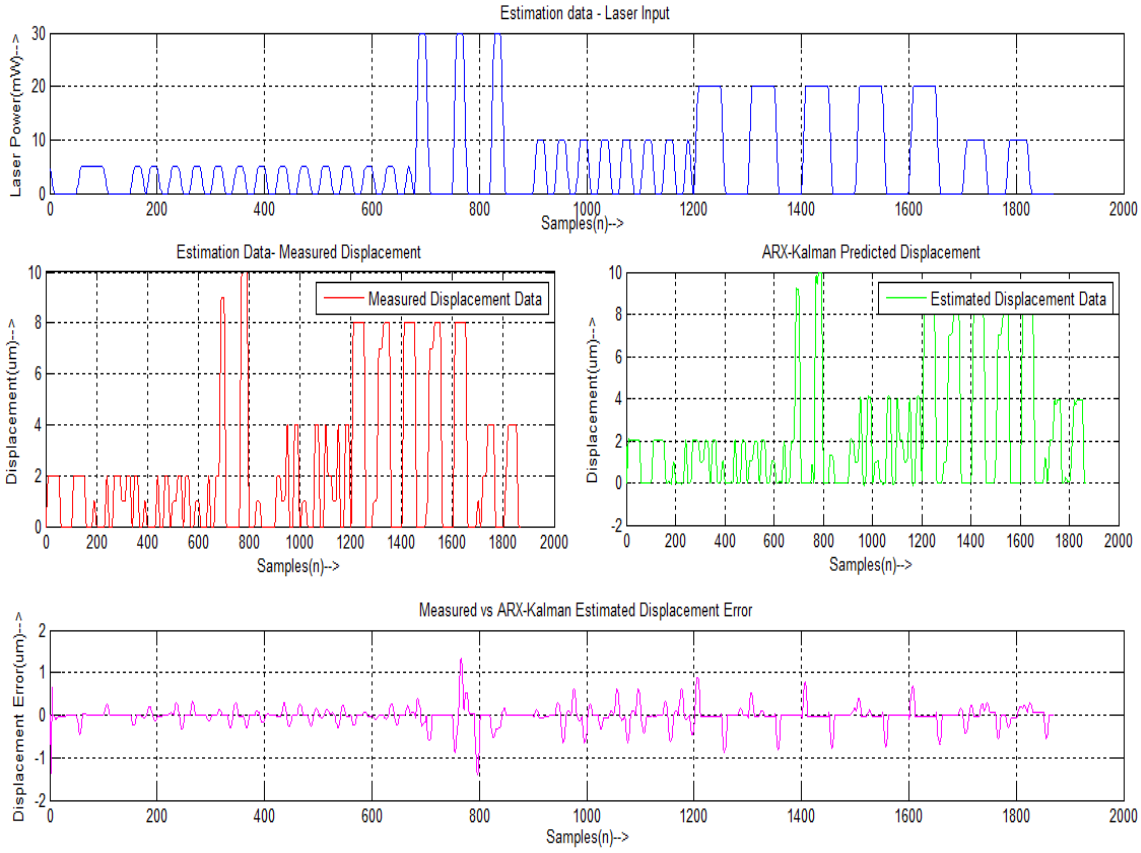

Figure 3.18 Kalman Predicted Vs. Measurement output from Estimation data with known I.C.

Model Validation:

As was explained before, we use system identification to validate the performance of the Recursive Kalman aided ARX model. The same validation model is used for comparing the performance of all the models. The figure below (fig. 3.19) shows the response of the system to the validation data. The parameters that are obtained at the end of the simulation for estimation data are used for initializing the prediction with the validation data. Similarly, the covariance matrix obtained at the end of simulation data prediction is used for initializing the predicting the validation data.

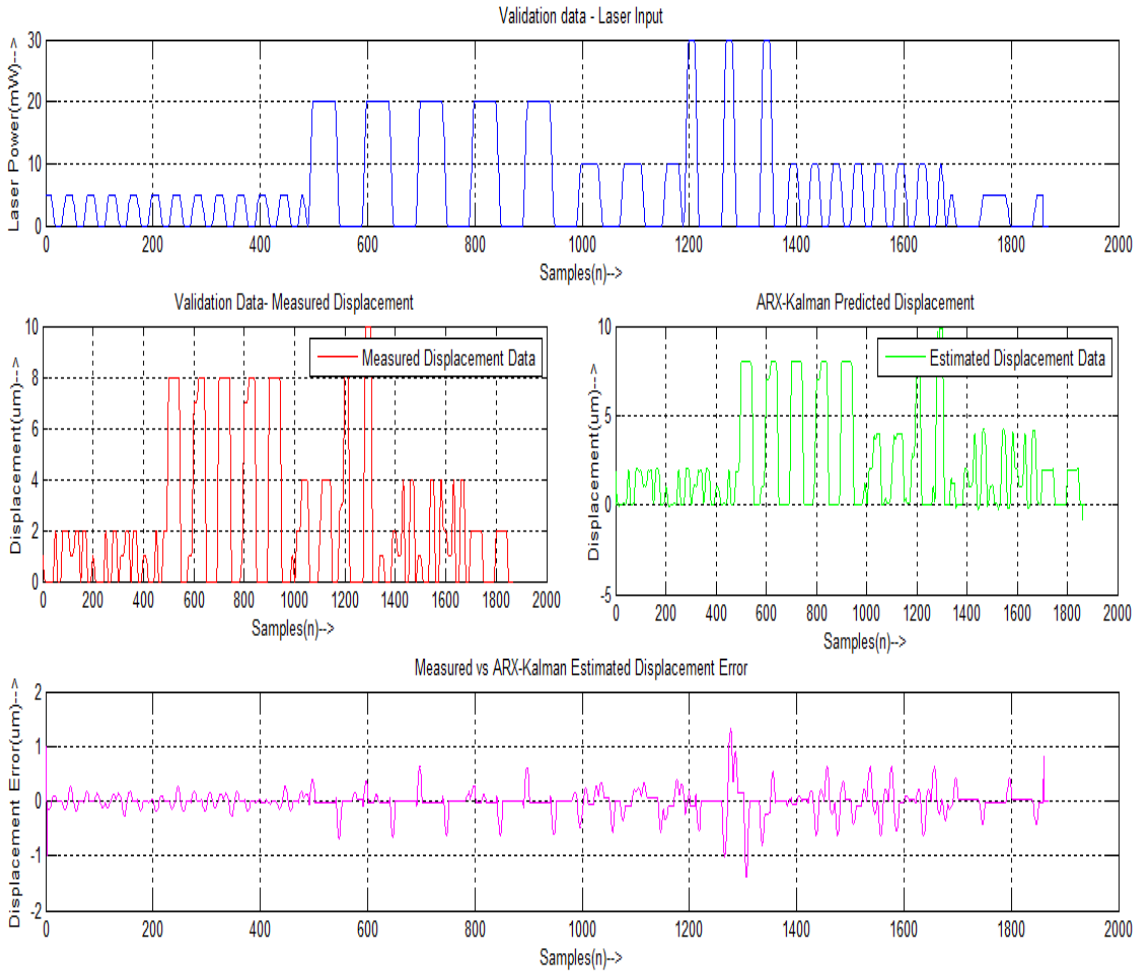

Figure 3.19 Kalman Predicted Vs. Validation Measurements with new I.C

The error plot (magenta) shown in subplot above shows that the error has the same performance characteristics as the error plot for the estimation data which implies that the parameters shows that the parameters obtained at the end of estimation are converge to real parameters values.

3.3.2 Recursive ARMAX with Kalman Filtering

Applying recursive Kalman filter to the ARMAX models defined below,

$$A(q)y(t) = B(q)u(t-nk) + C(t)e(t) \tag{3.12}$$

Where q is the delay operator.

$$A(q) = 1 + a_1 q^{-1} + a_2 q^{-2} + \ldots\ldots\ldots\ldots + a_{n_a} q^{-n_a} \tag{3.13}$$

$$B(q) = b_1 + b_2 q^{-1} + b_3 q^{-2} + \ldots\ldots\ldots\ldots + b_{n_b} q^{-n_b+1}$$

$$C(q) = 1 + c_1 q^{-1} + c_2 q^{-2} + \ldots\ldots\ldots\ldots + c_{n_c} q^{-n_c}$$

As done in the previous case for ARX models, we will apply recursive Kalman filter using parameter values obtained previously. Hence using the parameters derived in subsection 3.2.3 in eq. 3.8 for initial parameter values.

Model order = $[n_a\ n_b\ \ n_c\ \ n_k]$ = [1 2 5 0]

Initial Parameter Covariance Matrix = $P_0 = [\ldots]$

$$\begin{matrix} 0 & 0 & 0 & 0 & 0 & 0 & 0 & 0 \\ 0 & 0 & 0 & 0 & 0 & 0 & 0 & 0 \\ 0 & 0 & 0 & 0 & 0 & 0 & 0 & 0 \\ 0 & 0 & 0 & 0 & 0 & 0 & 0 & 0 \\ 0 & 0 & 0 & 0 & 0 & 0 & 0 & 0 \\ 0 & 0 & 0 & 0 & 0 & 0 & 0 & 0 \\ 0 & 0 & 0 & 0 & 0 & 0 & 0 & 0 \\ 0 & 0 & 0 & 0 & 0 & 0 & 0 & 0 \end{matrix}$$

Initial Parameter values= $[a_1\ b_1\ b_2\ c_1\ c_2\ c_3\ c_4\ c_5]$

$$= [0.1824\ \ 0.3448\ \ 0.02303\ \ 1.881\ \ 0.28\ \ -1.712\ \ -1.269\ \ -0.1583]$$

We are not yet sure of the initial covariance matrix which can be set to zero. Hence, applying recursive Kalman method to the estimation data as before, we obtain the following result shown in the figure below (fig. 3.20).

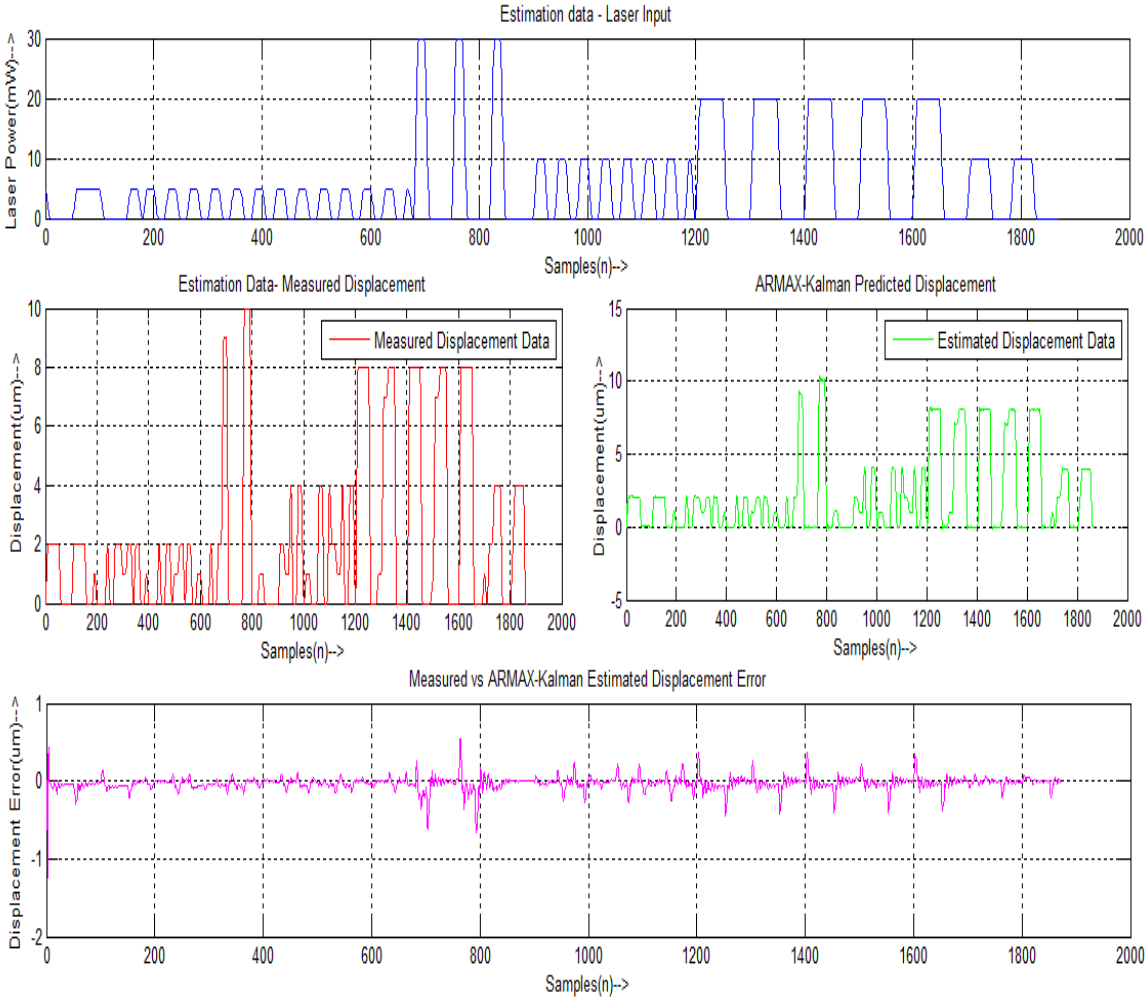

Figure 3.20 Kalman Predicted Vs. Measurement output from Estimation data with known I.C

The noise model has a predominant impact on the system which has much better approximation to the system noise. The parameter covariance matrix, predicted parameter values obtained at the end of the simulation are given below:

Final Covariance matrix P_N obtained,

0.0047	0.0017	-0.0005	-0.0001	0.0006	0.0009	0.0007	0.0006
0.0017	0.0085	-0.0079	0.0016	0.0043	0.0077	0.0057	0.0053
-0.0005	-0.0079	0.0080	-0.0020	-0.0047	-0.0081	-0.0060	-0.0055
-0.0001	0.0016	-0.0020	0.0403	0.0384	0.0408	0.0402	0.0222

0.0006	0.0043	-0.0047	0.0384	0.0664	0.0578	0.0582	0.0419
0.0009	0.0077	-0.0081	0.0408	0.0578	0.0715	0.0590	0.0441
0.0007	0.0057	-0.0060	0.0402	0.0582	0.0590	0.0679	0.0411
0.0006	0.0053	-0.0055	0.0222	0.0419	0.0441	0.0411	0.0433

Final Parameter values= $[a_1\ b_1\ b_2\ c_1\ c_2\ c_3\ c_4\ c_5]$

$$= [-0.9756 \quad 0.5185 \quad -0.5229 \quad 1.4070 \quad 1.9709 \quad 1.9566 \quad 1.3755 \quad 0.9825]$$

The error plot shown in the subplot (colored magenta) for fig.3.20 has very low error. At sample number 800, the error has reduced drastically compared to the error plots for ARX, ARMAX and recursive ARX models. This is one of the main advantages as the recursive ARMAX has the ability to comprise all the noise characteristics both known and unknown. Upon applying the parameter values obtained at the end of simulation to the validation data.

Model Validation:

As explained before for recursive ARX models we use the parameter values and the covariance values obtained at the end of estimation data to initialize the prediction with validation data. The prediction error subplot shown in figure below (fig. 3.21) is a clear indication of the performance of the recursive ARMAX model. The prediction error shown in fig.3.21 has much better performance characteristics which takes into account all the noise characteristics embedded in the form of laser beam reflection, camera reading error, algorithm's inaccurate video to displacement calculation, and other unexplained measurement noises.

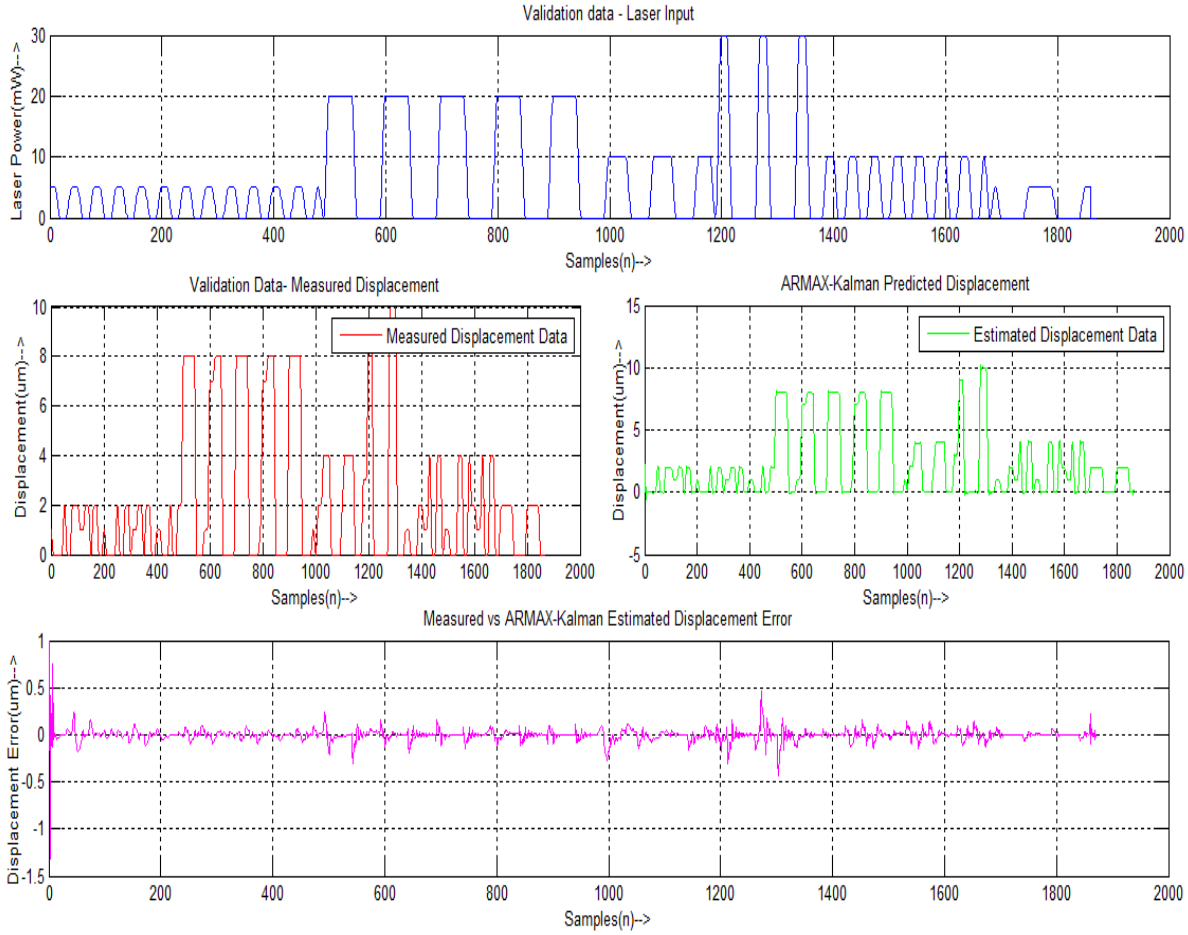

Figure 3.21 Kalman Predicted Vs. Validation Measurement output with new I.C.

3.4 Observation and Conclusion

We have performed several modeling and identification techniques with the experimental data obtained from the experiments in the above sections. For the non-recursive ARX model the prediction error was fluctuation in the range between [-20,20], while the non-recursive ARMAX model which was thought to produce better approximation seems to suffer from a prediction error in the range [-50, 50] which is more than expected. The prediction errors may have reduced by increasing the orders of the models but would have deviated from the expected order of the models. So, we still kept the orders of the models intact and applied the recursive methods for enhancing the parameters of the model.

The performance of the recursive models is clearly evident in the recursive ARX and ARMAX models in the above sections. The prediction error of the recursive ARX model has reduced to [-1, 1] from [-20, 20] which is a very drastic improvement. While for the recursive ARMAX model have a prediction error that ranges in [-0.5, 0.5] which is a significant improvement compared to the [-50,50] for the non-recursive ARMAX models.

This it can be concluded that the recursive ARX and ARMAX have better approximation to the actual physical laser actuated chevron actuator compared to the non-recursive models. The recursive ARMAX model which has better noise representation factors has much best approximation.

CHAPTER 4

SIMULATIONS OF LASER ACTUATED MICROROBOTS

4.1 Modeling of Laser Actuated Micro-robots

The modeling of laser actuated Chevrons is based on the thermal modeling of the system from the heat source. The heat source is the pulsed laser input source applied with a specified amplitude, beam width, pulse period and duty cycle. The parameters of the laser source can be varied and controlled but the laser source has a fixed wavelength which in turn is used for calculating the intensity of laser power applied.

The natural laser pulse characteristics with Gaussian distribution of intensity is used for modeling the distribution of intensity with change in position and point of application of the laser source is considered in order to mimic the behavior of actual laser actuated micro-robot.

In this section we describe the opto-thermo-mechanical equations used in modeling the system. The model is based on the equations defined in [35] by Pac and Popa**.** The equations describe the laser thermodynamics model equation which describe the thermal energy generation from the applied laser intensity. An analogical RC circuit model is taken into consideration to approximate the mechanical model of the micro-robot for to convert the thermal energy into kinetic energy. The force equations are used to approximate the displacement and orientation of the micro-robot. In this thesis, we will be discussing about the longitudinal displacement of the micro-robot as the orientation is highly non-linear.

The fig.4.1 describes the micro-robot which is modeled using Matlab and Simulink software.

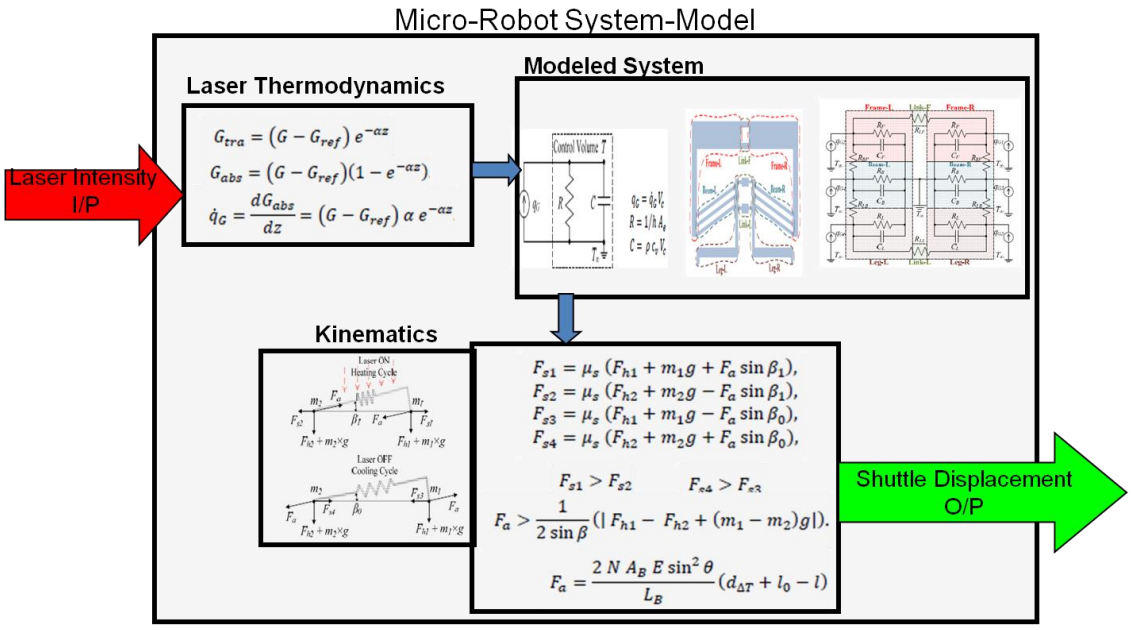

Figure 4.1 Schematic model of micro-robot modeled in Matlab and Simulink

4.2 Simulation Results and System Identification

The simulations results are obtained from a Simulink model with a variable time step hence the data has been assumed to be data samples approximated with 1ms sample time. The input to the model is a pseudo random input known to be the Laser source with a known Intensity given by $\frac{W}{m^2}$ while the output from the system is the position (in meters) of the micro-robot which changes with the input laser intensity. Below figure (fig. 4.2) contains the laser input and the corresponding output. Popa et. al. discuss dynamic modeling aspects for thermal bimorphs which will discuss on fitting appropriate system equations to inputs and output in [16].

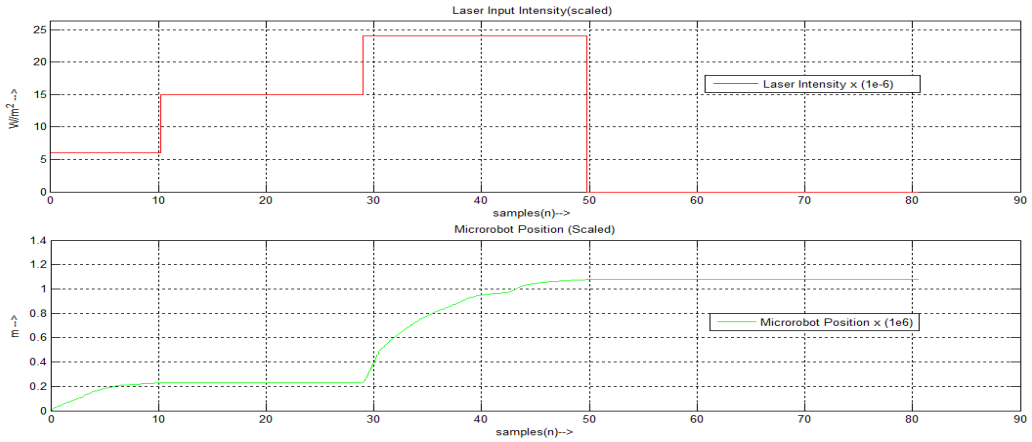

Figure 4.2 Laser Intensity (scaled) Vs. Robot Position (scaled)

The laser intensity which is of the order of $10^6 \frac{W}{m^2}$ and micro-robot position which is of the order of $10^{-6}\, m$ has been scaled down and plotted as shown in the figure (fig. 4.2). These scaled values will be used for system identification, as this reduces the computational overhead during system identification. From here-on, the manipulated data samples are scaled while their scaling factor will be denoted in figures and plots.

System Identification:

For the system identification, an appropriate combination of pseudo random data sample should be chosen. A combination of different experimental results from pseudo random data samples are combined to form the estimation data which will be used through-out this chapter for the purpose of system identification. The considered estimation data is a combination of 20 pseudo random experimental results, hence considering different estimation data for different identification models is not worthwhile. Similarly, a pseudo random combination of results from different experiments has been considered for validation. In this section we will not perform re-sampling process. Data obtained is from variable step model, a fixed sampled data is not possible to obtain. Based on simulation time and number of data points obtained, the data is equidistantly divided with one millisecond period.

We have already analyzed the behavior of linear and non linear models for system identification. But the use of recursive methods has provided to be more robust and adaptive to identify the system than all other models. Considering the use of control systems for future application which require a time varying adaptive observer models of physical systems, we will keep our focus more on recursive methods. Algorithm based on Kalman prediction method (discussed in previous chapter) will be used recursively calculating parameters with time, despite the disturbance from identified model or from external environment. Recursive methods applied to ARX and ARMAX model will be discussed in the following sections. Before performing system identification, we will analyze the nature of estimation data.

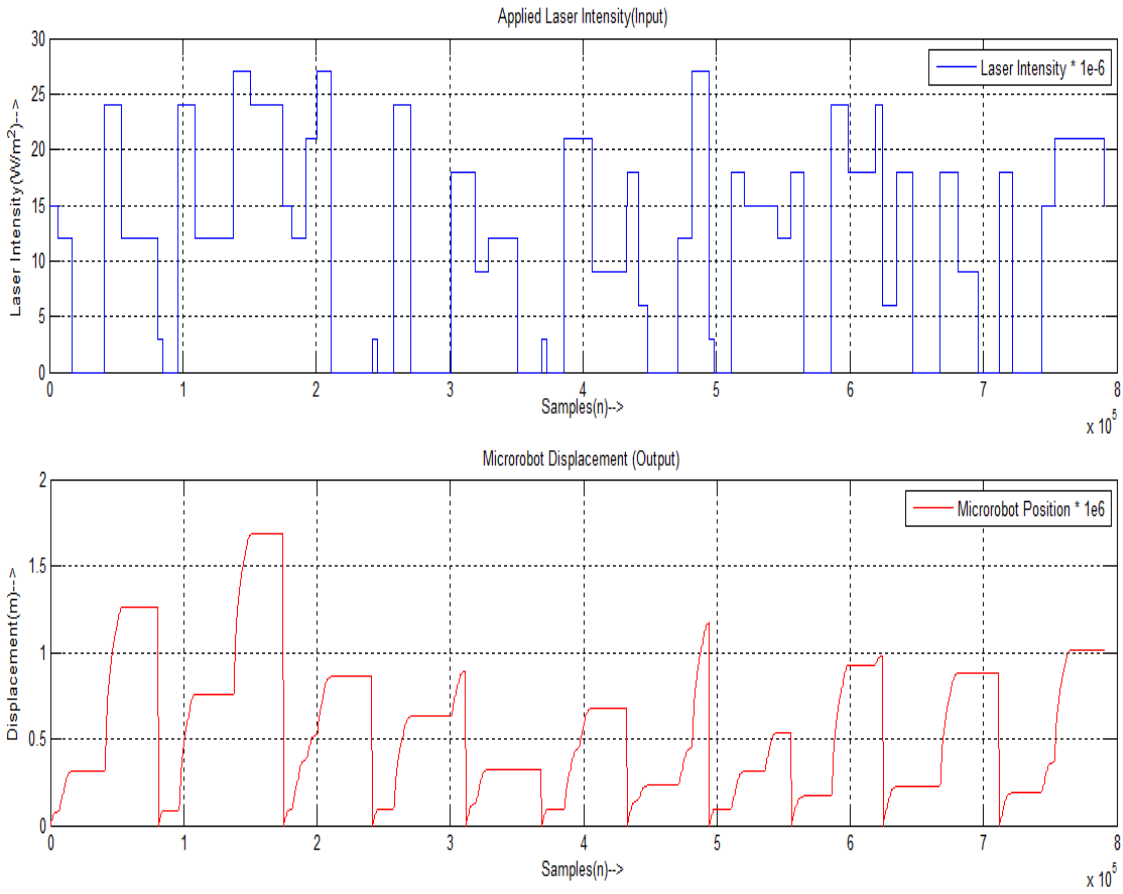

Figure 4.3 Estimation data – Input Vs. Output, both (scaled)

The estimation data obtained by stitching multiple data samples does not seem to be suffering from any random noise. Since the data is from a simulation model, we need not have to worry about the measurement noise from the camera or any other unexplained hardware error.

Since we have large number of data samples, the process of re-sampling (discussed in the previous chapter) is not performed. The system seems to highly non-linear and using adaptive techniques like recursive Kalman filtering.

4.2.1 Recursive ARX system Identification

Applying recursive ARX models defined below,

$$A(q)y(t) = B(q)u(t - nk) + e(t) \quad 4.1$$

Where q is the delay operator,

$$A(q) = 1 + a_1 q^{-1} + a_2 q^{-2} + \ldots\ldots\ldots\ldots + a_{n_a} q^{-n_a} \quad 4.2a$$

$$B(q) = b_1 + b_2 q^{-1} + b_3 q^{-2} + \ldots\ldots\ldots\ldots + b_{n_b} q^{-n_b+1} \quad 4.2b$$

We have checked the performance level of the recursive ARX models in the previous chapter and will be using the same method in predicting the parameter values of the system. We will be using a minimum order for the n_a and n_b.

The initial parameter and covariance values are unknown, hence we will initialize all the unknown parameter values and covariance matrix to zero.

Model order = $[n_a\ n_b\ n_k]$ = [2 2 1]

Initial Parameter Covariance Matrix = $P_0 = \begin{bmatrix} 0 & 0 & 0 & 0 \\ 0 & 0 & 0 & 0 \\ 0 & 0 & 0 & 0 \\ 0 & 0 & 0 & 0 \end{bmatrix}$

Initial Parameter values= $[a_1\ \ a_2\ \ b_1\ \ b_2]$ = [0 0 0 0]

Upon applying the estimation input to the initialized Kalman filter we obtain plot shown in the following figure (fig. 4.4). The subplot two (colored in red) and three (colored in green) are the estimation data and displacement data, respectively. The laser input plot and the

measurement plots are scaled for computational efficiency. The subplot (colored in magenta) is the displacement error which is the difference between measured to predicted displacement.

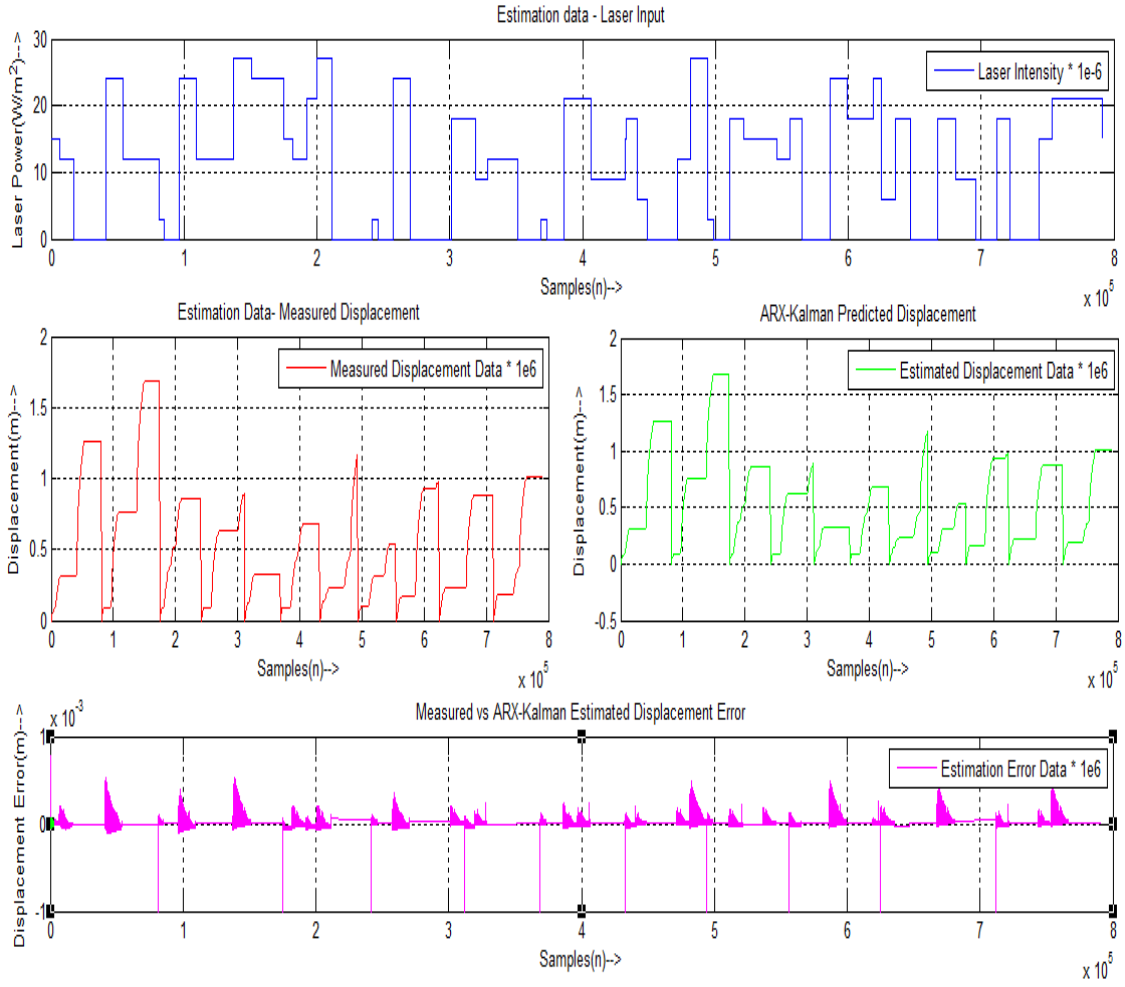

Figure 4.4 Kalman predicted Estimation data – Input Vs. Output, both (scaled)

The error subplot from the above figure (fig. 4.4) show sharp impulse at some discrete set of points. Since the estimation data is a combination of data from multiple experiments. Hence, the errors are a result of attaching discontinuous measurements points. These errors are acceptable as they have occurred at the same sample points where the data is discontinuous. The total prediction error is very low which implies that the parameter values estimated at the end of the simulation converge to the true parameter values of the actual

physical system. At the end of the simulation the estimated covariance matrix and the parameter values are shown below.

Parameter Covariance Matrix obtained at the end of simulation is given by,

$$P_N = \begin{bmatrix} 0.1005 & -0.1003 & 0.000 & 0.000 \\ -0.1003 & 0.1004 & -0.0000 & 0.0000 \\ 0.0000 & -0.0000 & 0.0001 & -0.0001 \\ -0.0000 & 0.0000 & -0.0001 & 0.0001 \end{bmatrix}$$

Parameter values= $[a_1 \;\; a_2 \;\; b_1 \;\; b_2]$ = [-1.0004 0.0029 0.0002 -0.0001]

As can be observed the Recursive ARX model has better performance in terms of keeping up with the measured outputs in terms of prediction. This improvement in performance is due to the error compensation factor ($\frac{1}{A(q)}e(t)$), as explained in the previous chapter.

Model Validation:

Apply parameter values, covariance matrix obtained at the end of previous simulations results with estimation data are applied as inputs for prediction with the validation data.

The figure below (fig. 4.5) shows the result of applying the recursive ARX to the validation data where we use the same color conventions as described before to denote the various subplots. The prediction error subplot is almost zero at all the points except for sharp impulses at discrete points which is a result of stitched data from multiple measurements. At this point the parameter values obtained at the end of the simulation data from fig. 4.4 are the true values of the actual physical system.

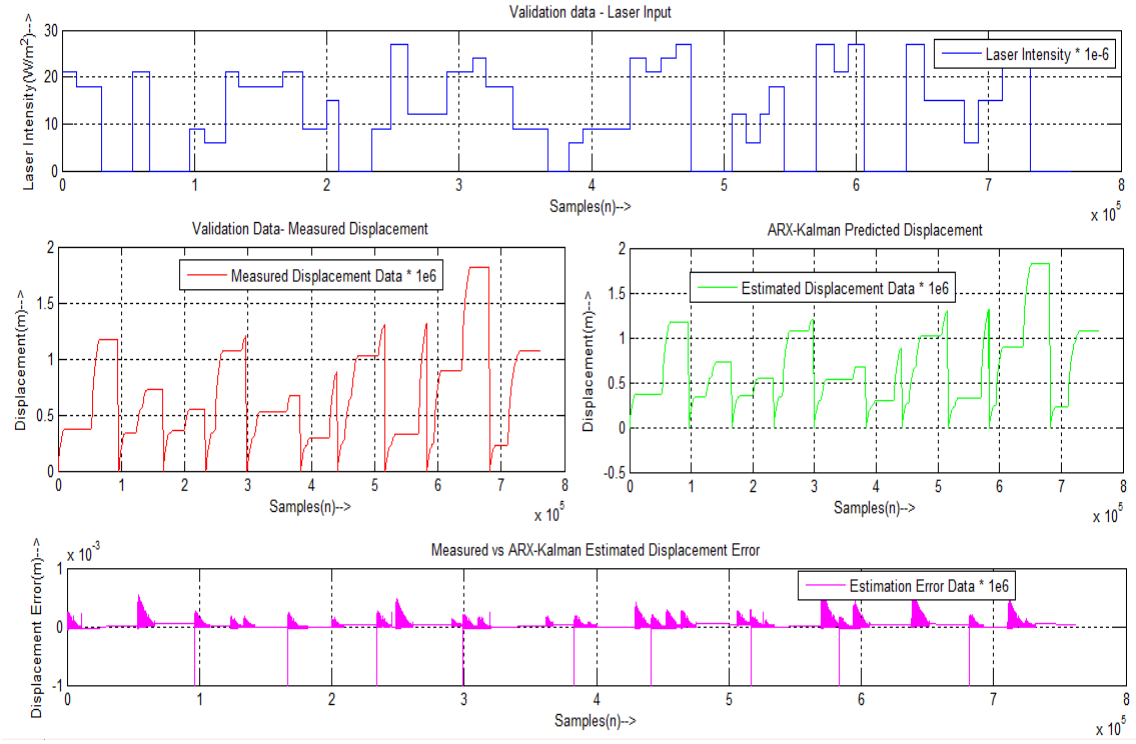

Figure 4.5 Measured Vs. Kalman Predicted Output for Validation data

4.2.2 Recursive ARMAX system Identification

Applying recursive ARMAX models defined below,

$$A(q)y(t) = B(q)u(t-nk) + C(t)e(t) \tag{4.3}$$

Where q is the delay operator,

$$A(q) = 1 + a_1 q^{-1} + a_2 q^{-2} + \ldots\ldots\ldots\ldots + a_{n_a} q^{-n_a} \tag{4.4}$$

$$B(q) = b_1 + b_2 q^{-1} + b_3 q^{-2} + \ldots\ldots\ldots\ldots + b_{n_b} q^{-n_b+1}$$

$$C(q) = 1 + c_1 q^{-1} + c_2 q^{-2} + \ldots\ldots\ldots\ldots + c_{n_c} q^{-n_c}$$

As done in the previous case for ARX models, we will apply recursive Kalman filter using parameter values obtained previously. Hence using the parameters derived in subsection 3.2.3 in eq. 3.15 for initial parameter values.

Model order = $[n_a\ n_b\ \ n_c\ \ n_k]$ = [1 2 5 0]

Initial Parameter Covariance Matrix = $P_0 = \begin{bmatrix} 0 & 0 & 0 & 0 & 0 & 0 & 0 & 0 \\ 0 & 0 & 0 & 0 & 0 & 0 & 0 & 0 \\ 0 & 0 & 0 & 0 & 0 & 0 & 0 & 0 \\ 0 & 0 & 0 & 0 & 0 & 0 & 0 & 0 \\ 0 & 0 & 0 & 0 & 0 & 0 & 0 & 0 \\ 0 & 0 & 0 & 0 & 0 & 0 & 0 & 0 \\ 0 & 0 & 0 & 0 & 0 & 0 & 0 & 0 \\ 0 & 0 & 0 & 0 & 0 & 0 & 0 & 0 \end{bmatrix}$

Initial Parameter values= $[a_1\ b_1\ b_2\ c_1\ c_2\ c_3\ c_4\ c_5]$

$= [0.1824\ \ 0.3448\ \ 0.02303\ \ 1.881\ \ 0.28\ \ -1.712\ \ -1.269\ \ -0.1583]$

We are not yet sure of the initial covariance matrix which can be set to zero. Hence, applying recursive Kalman method to the estimation data as before, we obtain the following result shown in figure below (fig. 4.6).

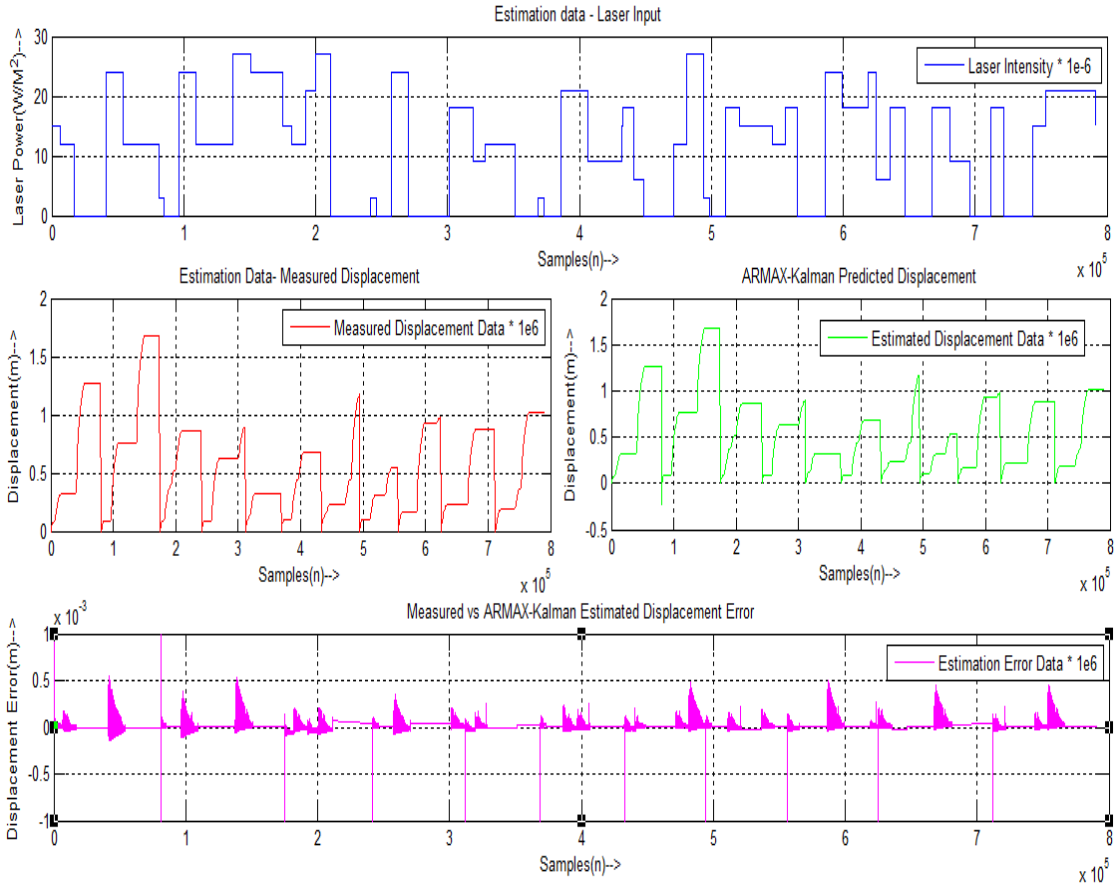

Figure 4.6 Measured Vs. Kalman Predicted Output for Estimation Data

The noise subplot from the above figure (fig. 4.6) has the same characteristics as explained in the previous section for recursive ARX model. The impulses are due to the discontinuous data points from different experiments.

Final Covariance matrix P_N obtained,

0.0047	0.0017	-0.0005	-0.0001	0.0006	0.0009	0.0007	0.0006
0.0017	0.0085	-0.0079	0.0016	0.0043	0.0077	0.0057	0.0053
-0.0005	-0.0079	0.0080	-0.0020	-0.0047	-0.0081	-0.0060	-0.0055
-0.0001	0.0016	-0.0020	0.0403	0.0384	0.0408	0.0402	0.0222
0.0006	0.0043	-0.0047	0.0384	0.0664	0.0578	0.0582	0.0419
0.0009	0.0077	-0.0081	0.0408	0.0578	0.0715	0.0590	0.0441
0.0007	0.0057	-0.0060	0.0402	0.0582	0.0590	0.0679	0.0411
0.0006	0.0053	-0.0055	0.0222	0.0419	0.0441	0.0411	0.0433

Final Parameter values= $[a_1\ b_1\ b_2\ c_1\ c_2\ c_3\ c_4\ c_5]$

$$= [-0.9756 \quad 0.5185 \quad -0.5229 \quad 1.4070 \quad 1.9709 \quad 1.9566 \quad 1.3755 \quad 0.9825]$$

Model Validation:

We use the same validation data as explained before for prediction using the Kalman aided ARMAX model. The parameter values are initialized from the final parameter values obtained from values at the end of simulation results for estimation data. The covariance matrix is also obtained from the finally calculated covariance matrix obtained at the end of the simulation with estimation data. The error plot shows a sharp improvement as the error is completely zero expect for the sharp impulses due to the discontinuous data sets made from multiple datasets.

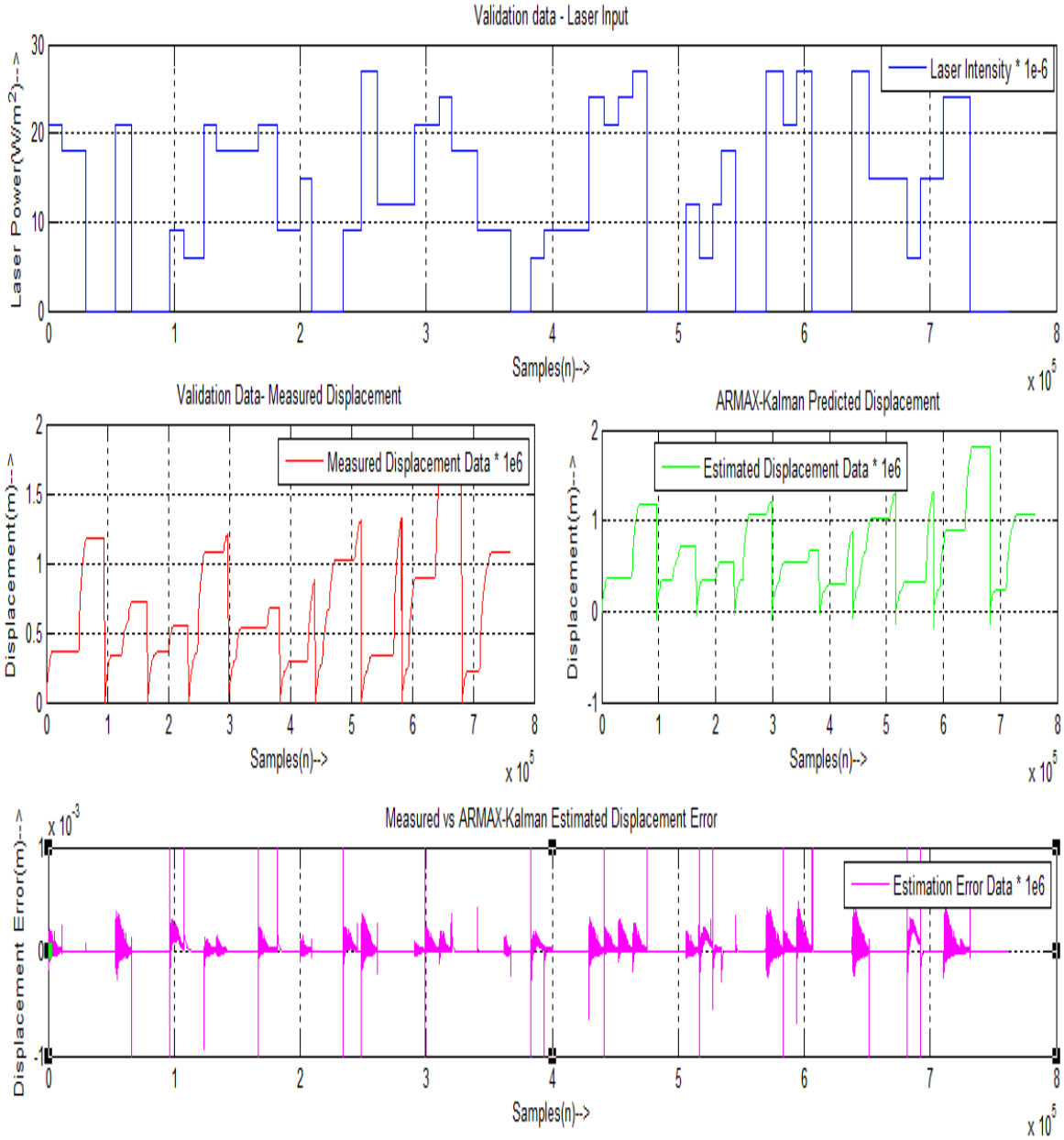

Figure 4.7 Measured Vs. Kalman Predicted Output for Validation data

Both recursive ARX and ARMAX have better parameter approximation characteristics in parameter estimation.

4.3 Observations and Conclusions

We had already observed and concluded the capability of recursive models over non-recursive models in the chapter 3. In this chapter, instead of repeating the non-recursive models followed by recursive models we have directly jumped into using recursive models. As we can observe in fig. 4.4 for recursive ARX model and fig 4.6 for recursive ARMAX model, both seems to have better approximation to the actual physical models with the prediction error almost zero. The sharp impulses are not accountable in the prediction error as the validation data and estimation data has been prepared from multiple discontinuous experiments. Hence, we can say that the recursive models have better approximation compared to the actual physical system.

CHAPTER 5

ELECTROTHERMALLY ACTUATED CHEVRON ACTUATORS

5.1 Modeling of Electro-thermally actuated Chevron Actuators

In this chapter we will discuss about the electro-thermally actuated Chevron actuators. These are the experiments performed at the Veeco station where the source of input is from automated voltage source. Veeco uses interferometer techniques to measure the displacement in the Chevron centre shuttle for an applied input voltage. The nature of the applied input is a square wave at different frequencies with zero phases. Hence, the measurement data consist of 2-D table or graph consisting of frequency versus displacement. The phase characteristics are not considered for identification. The figure below (fig. 5.1) shows the amplitude frequency versus displacement plot of one such experiment conducted at Veeco. The details of the experiment are mentioned in chapter 1.

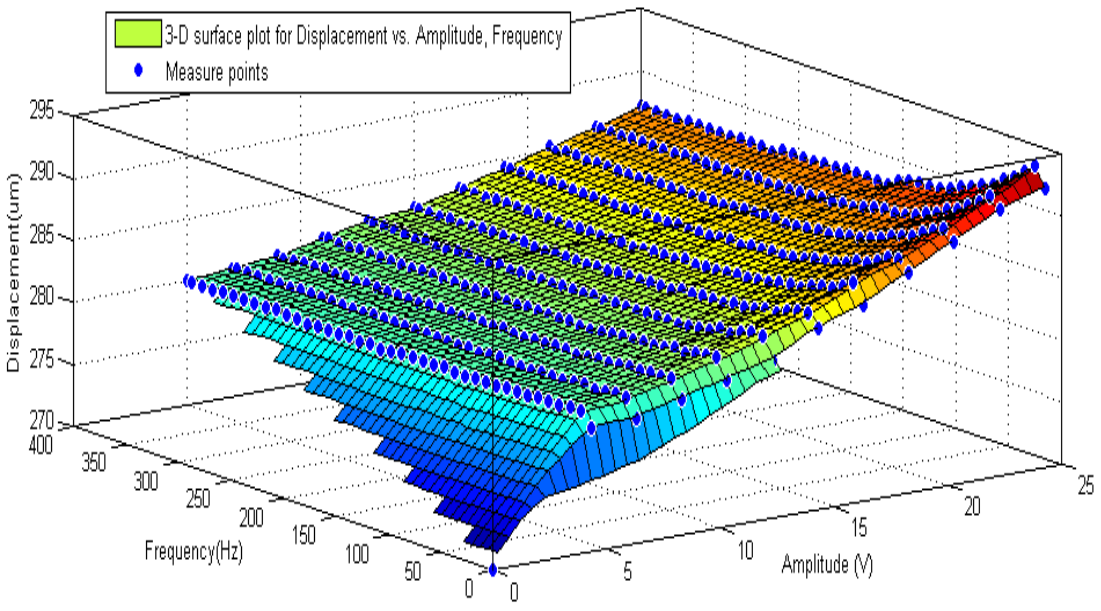

Figure 5.1 Amplitude, Frequency Vs. Displacement plot

5.2 Re-Sampling and curve fitting

The experimental data consists of applying a square wave with a fixed amplitude while varying frequency from 0 to 400 Hz. The experiment has been repeated for amplitudes ranging from 0 to 25V. The frequency resolution of the experimental data is 10Hz while the amplitude resolution is 2V. These data samples are insufficient for performing curve fitting and we discussed about this scenario in previous chapters. In order to compensate for the insufficient data samples we use a curve fitting method for fixing a three dimensional surface.

As discussed in previous chapter, we use the curve fitting toolbox from MATLAB to fit a three dimensional surface to the existing data samples. Three dimensional interpolants are used for surface fitting to the existing data samples. The interpolants work by breaking the data samples into multiple segments and try to fix a surface to the individual segments.

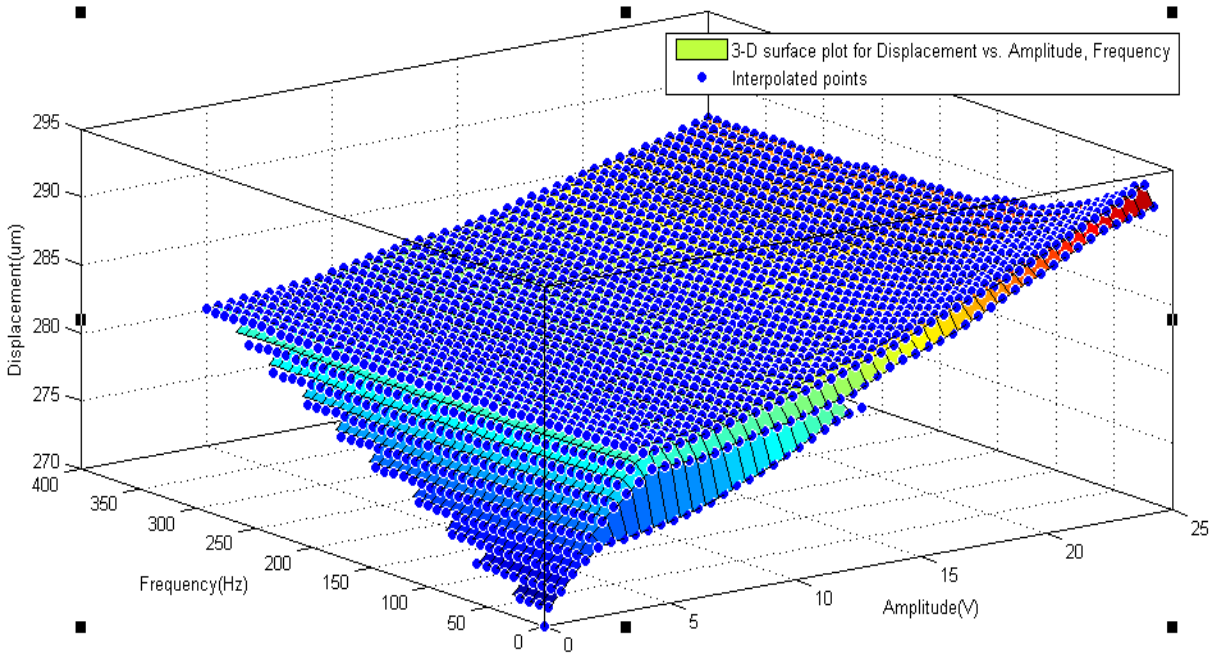

Figure 5.2 Interpolated surface fitted Amplitude, Frequency Vs. Displacement plot

Surface fitting accuracy increases with the number of interpolants used and the number of data samples. Since we have limited data samples, we use more interpolants to fit the best

surface. The figure above (fig. 5.2) shows the fitted surface with interpolated data samples where the amplitude has a resolution of 0.1 V while the frequency has a resolution of 1 Hz.

Now having sufficient number of measured and interpolated data samples we start the procedure for system identification which will be explained in the next subsection.

5.3 Polynomial surface fitting for shuttle displacement

Having sufficient number of data samples, we use the surface fitting method to fix generic 3-D polynomial to comprise the entire frequency and amplitude range of chevron actuator.

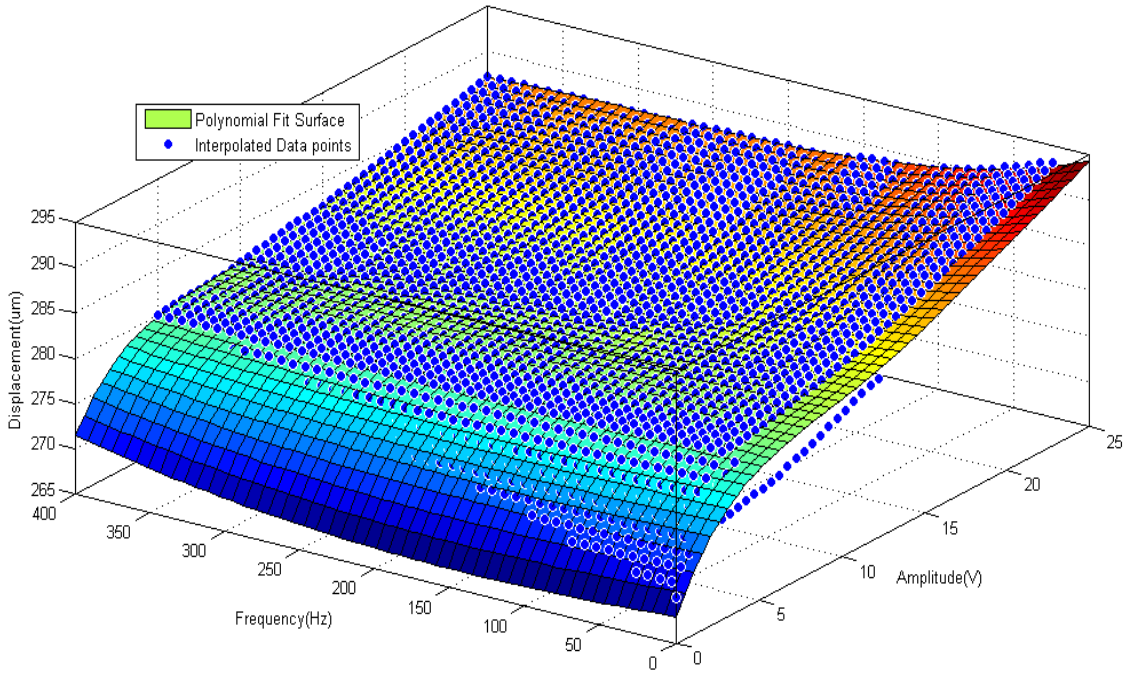

Figure 5.3 3-D polynomial surface fitted Vs. data samples

Using MATLAB, we fit a surface polynomial to the data points. The equation below shows the 3-D polynomial surface fitted.

$$f(x,y) = 267.9 + 4.359.x - 0.01172.y - 0.5892.x^2 + 0.003353.x.y + 0.000032.y^2 + 0.04129.x^3 - 0.000359.x^2.y - 0.001318.x^4 \quad 5.1$$

The figure above (fig. 5.3) shows the surface plot of the above equation versus the data samples which can be used to compare the fitted surface to the data samples. The accuracy of the surface fit is given by term R-square which is 99.30%. The R-square term is the correlation term which measured the convergence of data samples to the polynomial surface. The polynomial fit is performed using linear least squares method. The cumulative root mean square error is given by 0.1327.

5.4 Force measurement from chevron shuttle

In Fig. 1.7, we explained the setup for measuring the force produced by the chevron shuttle for the corresponding input voltage using the force sensor. The force sensor is placed right in front of the shuttle and with the applied voltage across the terminals of the chevron actuator, the shuttle displaces. The displaced shuttle applied considerable force upon the sensor to make a measurement. As mentioned before a forces sensor from Kronex Corporation called AE 801 is used for taking the measurement from the chevron actuators. A random set of inputs voltages are applied to the chevron actuator and the corresponding force measurement embedded in voltages measurement of sensor is saved. The process is repeated for the entire number of samples. The plots shown in the figure (fig. 5.5) below displays the applied voltage input to the chevron actuator and the corresponding voltage reading from the sensor. A comprehensive discussion of force measurements is discussed in [40] by Miche and Ehrfeld with prime focus on micro gear pumps, actuators, miniaturized clamping requirements for wide range of applications.

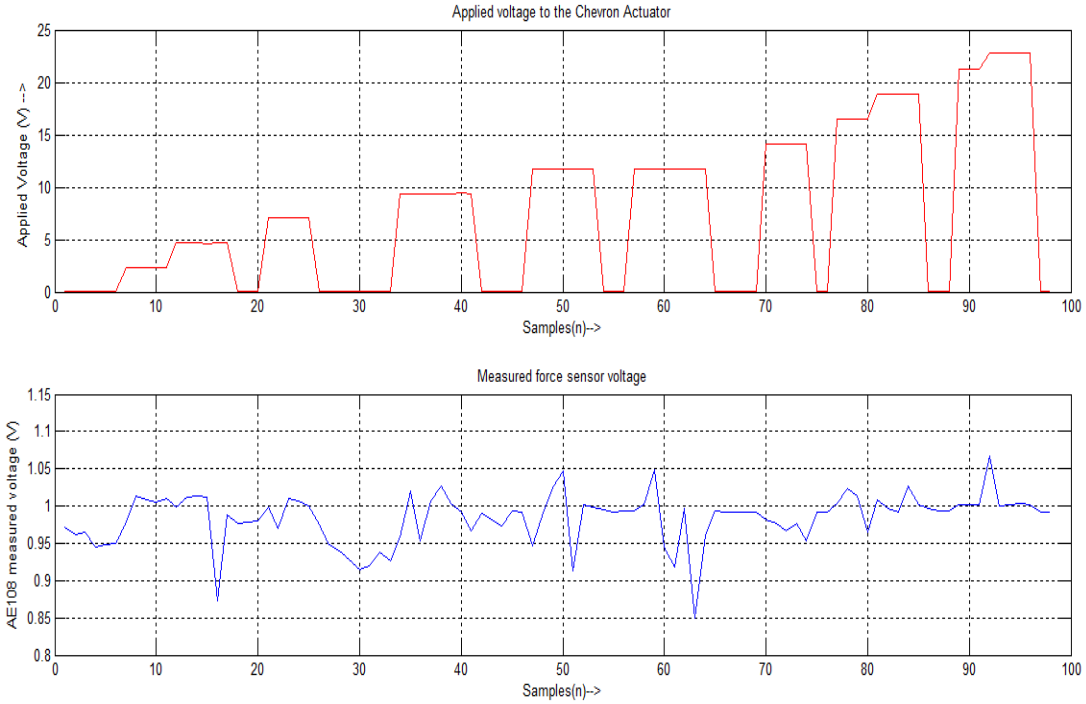

Figure 5.4 Applied Chevron actuation voltage Vs. force sensor voltage reading

The following equations define the characteristic relation between the measured sensor voltage to the actual force measurement. The equation relating deflection of the force sensor to measured voltage is given by

$$\mathrm{d} = \frac{\Delta \mathrm{U}.\mathrm{l}^3}{0.75.\mathrm{U}.\gamma.(\mathrm{l}-0.5).\mathrm{h}} \qquad 5.2$$

Where

d = Deflection of the sensor; ΔU=measured sensor voltage; l =sensor length;

γ = sensor resistors Gauge number; h=width of the sensor.

The calculated displacement of the force sensor to the force generated by the shuttle beam is given by the equation below.

$$F = C.d \qquad 5.3$$

Where, F=force generated by the shuttle; C=stiffness constant of the sensor;

d=calculated sensor displacement due to the force generated by the chevron beam.

Using the above two equations with sensor measurement voltage, we can calculate the actual force experienced by the sensor due to the force generated by the chevron shuttle for the applied voltage across its terminals.

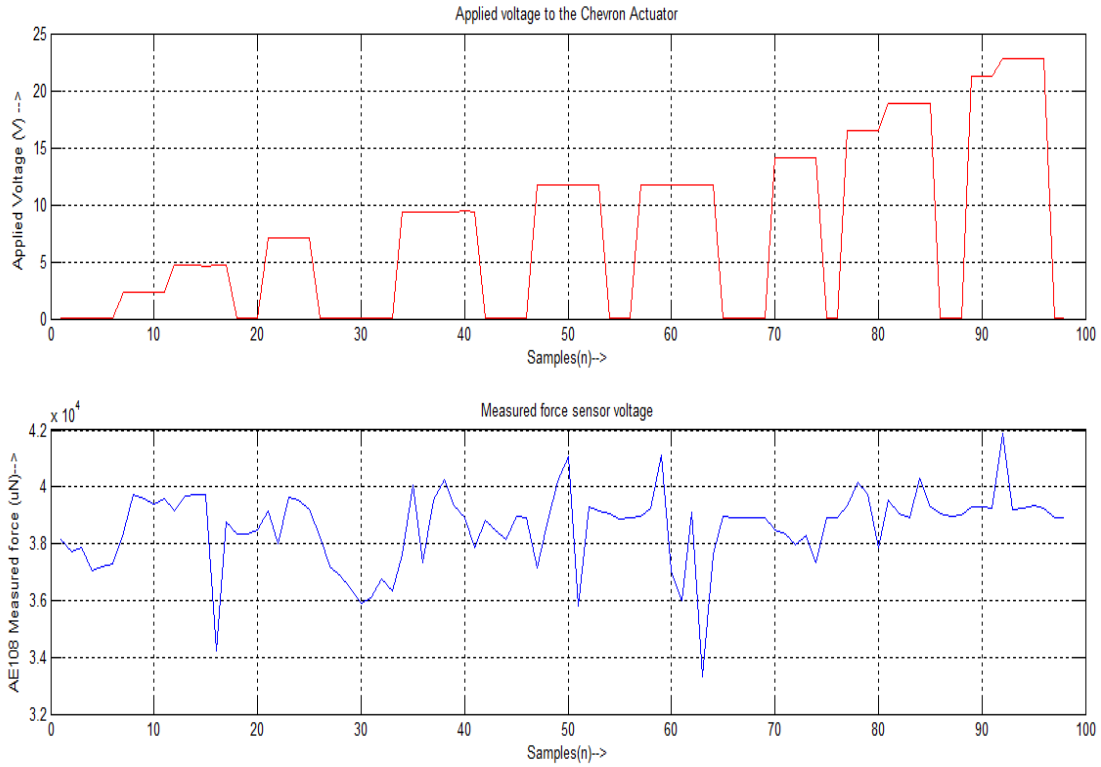

Figure 5.5 Applied Chevron actuation voltage Vs. force generated from sensor reading

From the above figure (fig. 5.5) it can observed that the measurement for the same applied voltage are having different measurements in the successive measurements. Hence finding the average sensor measurement for the applied voltage we obtain the following plot as shown below.

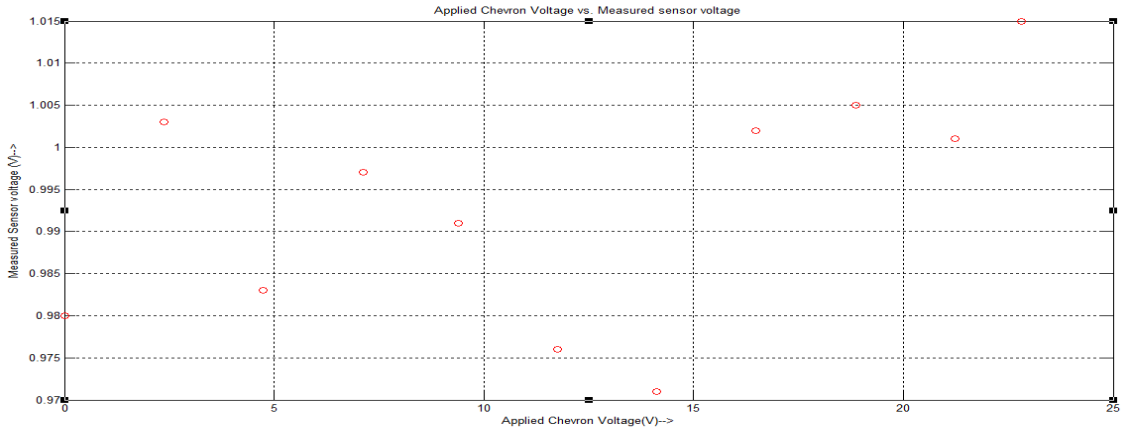

Figure 5.6 Applied average chevron actuation voltage vs. average sensor reading

From the above figure (fig. 5.6), converting the average measured sensor voltage into force using eq. 5.2 and eq. 5.3 we obtain the plot shown in the figure below (fig. 5.7).

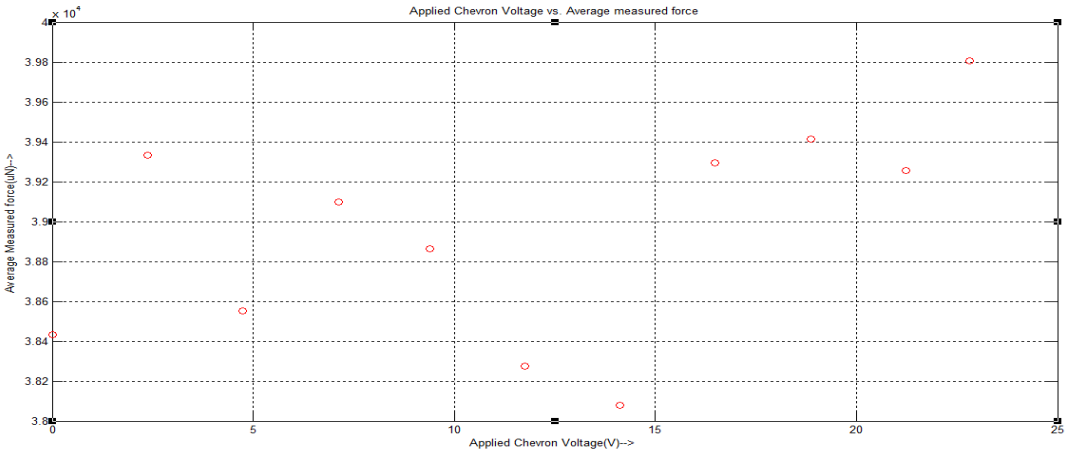

Figure 5.7 Applied average Chevron actuation voltage Vs. average force measured

Using Matlab Curve fitting toolbox, we obtain the curve shown below given in eq. 5.4.3.

$$f(x) = P_1.x^8 + P_2.x^7 + P_3.x^6 + P_4.x^5 + P_5.x^4 + P_6.x^3 + P_7.x^2 + P_8.x^1 + P_9 \quad 5.4$$

$$P_1 = -0.0001253$$

$$P_2 = 0.01251$$

$$P_3 = -0.5104$$

$$P_4 = 10.93$$

$$P_5 = -131$$

$$P_6 = 868.9$$

$$P_7 = -2919$$

$$P_8 = 3866$$

$$P_9 = 3.841e + 004$$

where x is the applied chevron voltage and f(x) is the average measured force generated by the chevron shuttle on the sensor. The figure below (fig. 5.8) shows the plot of the Measured average force points by the sensor and the eighth order polynomial fit curve.

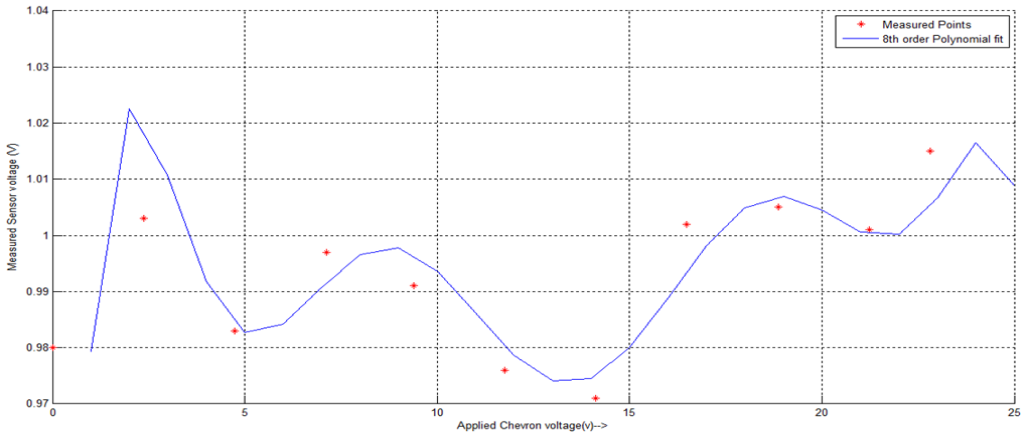

Figure 5.8 Measured data points Vs 8th order polynomial fit.

The above derive non-linear 8th order polynomial may be an appropriate fit to the measured data points. The data points may have been suffering with measurement inaccuracies. A linear 2nd order as shown below is the appropriate fit to define the force generated by the chevron actuator shuttle for the applied input voltage.

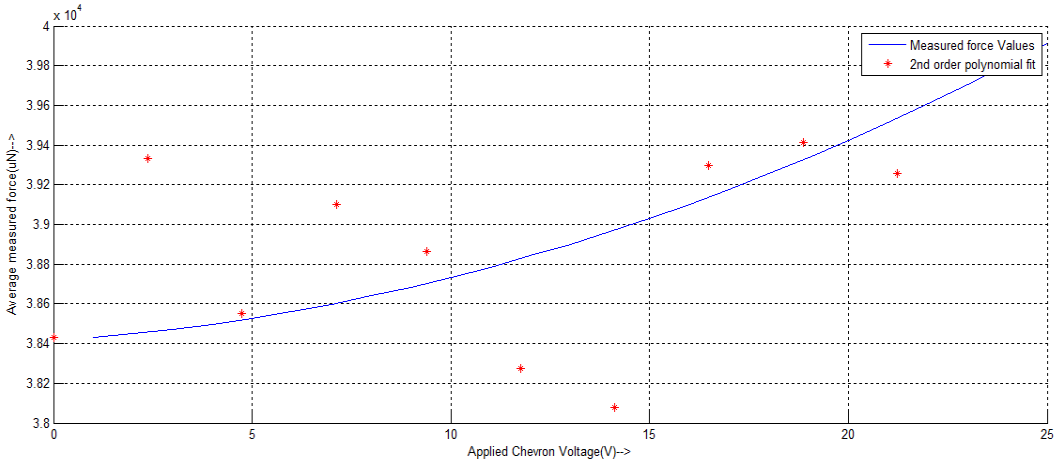

Figure 5.9 Measured data points Vs 2nd order polynomial fit.

$$f(x) = P_1.x^3 + P_2.x^2 + P_3 \qquad 5.5$$

$$P_1 = 1.885$$

$$P_2 = 16.44$$

$$P_3 = 3.843\text{e}+004$$

Where f(x) is the measured force generated by the chevron shuttle, x is the applied voltage across the chevron actuator.

The force generated from micro-actuators have typical applications as discussed in [41] by Pakkratok, Luekiatphaisan and Aoyama where a piezo and voice call actuators are used for testing hardness and stiffness of other micro-robots. These micro-actuators play a crucial role in deciding the quality of the manufactured micro structures.

5.5 Observation, Conclusions and Applications

In this chapter, we have established the relationship between the applied voltage across the chevron actuator, with a particular amplitude and frequency to the displacement of the shuttle beam. Since the experiments are actually performed at the Veeco work station which has the added advantage to conducting the experiments in automation. We were able to apply the inputs such as square waves or sine waves with a desired amplitude and frequency and

observe the displacement measurements of the chevron shuttle. The frequency plot of the non-recursive ARX and ARMAX from chapter 3 seems to have the same frequency characteristics as shown in the fig. 5.3 identified by eq. 5.1. Thus even though the actuation inputs applied are different the characteristics of the identified models are the same.

The force measurements play an important role in the design of micro-robots. The equations used in chapter 4 for designing the micro-robot model were based on these force equations for the actuation forward motion of the entire micro-robot. The paper by Muhammed R. Pac and Dan O. Popa in [35] details about these force equations used and their role in actuation motion of the micro-robot. Even though, the experimental data collected for force measurements from force sensor seems to be suffering from wide deviations due to the sensor strain characteristics. The availability of highly precise force measurement sensors will reduce the measurement deviation thus increasing the accuracy of the measurement. Eventually the force measurements will have to approximate to eq. 5.5 to bring the relationship between the applied voltage input and chevron generated shuttle measurements.

CHAPTER 6

CONCLUSIONS AND FUTURE WORK

6.1 Conclusions

As specified in Chapter 1 regarding the future scope and applications of this thesis, there are some important conclusions that should be drawn from the experiments performed and corresponding mathematical models calculated in the all the chapters 3,4 and 5.

In chapter 3, the experiments on laser actuated Chevron actuators play the crucial role in deriving the experimental data for system identification. The experimental data is further used for model fixing and system identification to derive the appropriate model. As shown in fig.1.2, a hypothetical micro-robot made of multiple chevron type actuators can be modeled using the different mathematical models derived in Chapter 3 for the displacement generated by each leg of the robot due to the applied laser power.

Similarly, the mathematical models created in chapter 5 for electro-thermally actuated chevron are used for creating micro-robots where each leg of the micro-robot is actuated with the applied voltage source. The force equations derived play an important role in deriving the kinematic motion of the micro-robot produced by each leg.

In chapter 4, we came across a laser actuated micro-robot which was designed and manufactured using the thermodynamic and kinematic equations. The entire micro-robot was modeled as a RC circuit model to perform simulation and derive the appropriate mathematical relationship between the applied laser intensity and the displacement. A careful observation shows that the force equations used in kinematic motion of micro-robot are similar to the force relation that was derived in chapter 5 for electro-thermally actuated Chevrons.

Summarizing the above said, the experiments performed and the mathematical relationship obtained we had finally justified the scope of the thesis.

6.2 Future work

System identification plays an important role in control systems applications. The future scope of this thesis is to apply control systems to micro-robots created from multiple micro-actuators. Since we already have a mathematical model that describe the characteristic response of the micro-actuators (Chevron actuators, in this thesis), we can derive the mathematical model of entire micro-robots which are designed depending on applications.

REFERENCES

[1] D.O. Popa, “Microactuators”, in Encyclopedia of Micro and Nano Fluidics, ed. D. Springer, 2008.

[2] Lyshevski, S.E.; Lyshevski, M.A., “Analysis, dynamics, and control of micro-electromechanical systems”, American Control Conference, 2000. Proceedings of the 2000.

[3] D. O. Popa, et. al., “Computationally Efficient Dynamic Modeling of MEMS”, in Proc of 7-th Int’l Conf. on Modeling and Simulation of Microsystems, March 2004.

[4] Bryzek, J., Abbott, H; Flannery, A.; Cagle, D.; Maitan, J. “Control issues for MEMS”, Decision and Control, 2003. Proceedings. 42nd IEEE Conference.

[5] B. Borovic, F. L. Lewis, D. Agonafer, E. S. Kolesar, M. M. Hossain, D. O. Popa, Method for Determining a Dynamical State-Space Model for Control of Thermal MEMS Devices, Journal of Microelectromechanical Systems, Vol. 14, Issue 5, Nov. 2005.

[6] B. Borovic, A.Q. Liu, D. O. Popa, H. Cai, and F.L. Lewis “Open-loop vs closed-loop control of MEMS devices: choices and issues,“ in Journal of Micromech. Microeng. 15 (2005) 1917 1924.

[7] D.O. Popa, H. E. Stephanou, “Micro and Meso Scale Robotic Assembly”, in SME Journal of Manufacturing Processes, vol. 6 No. 1, 2004, 52-71.

[8] Loizou, S.G., Kyriakopoulos, K.J. , “Motion Planning of Piezoelectrically Driven Micro-Robots Via Navigation Functions”, Intelligent Control, Proceedings of the 2005 IEEE International Symposium on, Mediterrean Conference on Control and Automation.

[9] R. Murthy, A.N.Das, D. O. Popa, “ARRIpede: A Stick-Slip Micro Crawler/Conveyer Robot Constructed Via 2 ½D MEMS Assembly,” in Proc. of 2008 IEEE Int’l Conf. on Intelligent Robots and Systems (IROS ’08), Nice, France, Sept. 22-26, 2008.

[10] R. Murthy, D.O. Popa, “Articulated MEMS Robot for Microfactory Applications,” in Proc. of ASME IDETC’09, Micro-Nano Systems Conference (MNS), San Diego, CA, August 30-September 2, 2009.

[11] R. Murthy, D.O. Popa, “Nonholonomic Control for an Assembled Microcrawler,” in Proc. of 9th IFAC Symposium on Robot Control, Gifu, Japan, September 9-12, 2009.

[12] R. Murthy, D. O. Popa, “A Four Degree Of Freedom Microrobot with Large Work Volume”, in proc. of IEEE ICRA ‘09, Kobe, Japan, May 2009.

[13] R. Murthy, A.N. Das, D. O. Popa, “Multiscale Robotics Framework for MEMS Assembly,” in Proceedings of the Ninth International Conference on Control, Automation, Robotics and Vision (ICARCV), Singapore, Dec 2006.

[14] K. Rabenorosoa, A.N. Das, R. Murthy, C. Clevy, D.O. Popa, P. Lutz, " Precise Motion Control of a Piezoelectric Microgripper for Microspectrometer Assembly," in Proc. of ASME IDETC'09, Micro-Nano Systems Conference (MNS), San Diego, CA, August 30-September2, 2009.

[15] Kole, A.; Jeongsik Sin; Woo Ho Lee; D. O. Popa; Agonafer, D.; Stephanou, H.;" Design of polymer tube embedded in-plane micropump," Thermal and Thermomechanical Phenomena in Electronics Systems, 2006. ITHERM '06. The Tenth Intersociety Conference on May 30-June 2, 2006 Page(s):1324 – 1329.

[16] Popa, D.O.; Kang, B. H.; Wen, J.T.; Stephanou, H.E.; Skidmore, G.; Geisberger, A.;,"Dynamic Modeling and Open-Loop Control Of Thermal Bimorph MEMS Actuators," in Proc. IEEE Conf. on Robotics and Automation, Taipei, Taiwan, 2003.

[17] M.A. Mayyas, W.H. Lee, D.O. Popa, P. Shiakolas, P. Zhang, H. E. Stephanou,"Comprehensive Electrothermal Modeling of a Thermal Microgripper," TEXMEMS VII International Conference on MEMS, El Paso, TX, September 2005.

[18] Gensler, H., Sheybani, R.; Po-Ying Li; Lo, R.; Zhu, S.; Ken-Tye Yong; Roy, I.; Prasad, P.N.; Masood, R.; Sinha, U.K.; Meng, E. "Implantable MEMS drug delivery device for cancer radiation reduction", Micro Electro Mechanical Systems (MEMS), 2010 IEEE 23rd International Conference.

[19] D. O. Popa, et. al., "Dynamic Modeling and Input Shaping for MEMS", in Proc of 7-th Int'l Conf. on Modeling and Simulation of Microsystems, March 2004.

[20] Saif, M.T.A.; Alaca, B.E.; Sehitoglu, H., " Analytical modeling of electrostatic membrane actuator for micro pumps" Journal of Microelectromechanical Systems.

[21] Bou, D.I.S.; Almansa-Martin, A. "Study on micro handling and assembly methods and tools within the project ASSEMIC", Industrial Technology, 2004. IEEE ICIT '04. 2004 IEEE International Conference.

[22] B. Floyd, S.; Pawashe, C.; Sitti, M.," An untethered magnetically actuated micro-robot capable of motion on arbitrary surfaces" Robotics and Automation, 2008. ICRA 2008. IEEE International Conference.

[23] M Lu Ren; Lidai Wang; Mills, J.K.; Dong Sun "3-D automatic microassembly by vision-based control",Intelligent Robots and Systems, 2007. IROS 2007. IEEE/RSJ International Conference.

[24] Rabenorosoa, K.; Clevy, C.; Lutz, P.; Bargiel, S.; Gorecki, C., "A micro-assembly station used for 3D reconfigurablehybrid MOEMS assembly",Assembly and Manufacturing, 2009. ISAM 2009. IEEE International Symposium.

[25] Green, A.A.; Qing Hua Wang; Hersam, M.C., "Chemically tailored carbon-based nanoelectronic materials and devices ", Nanotechnology, 2009. IEEE-NANO 2009. 9th IEEE Conference.

[26] Dang, P., Lewis, F. L., Subbarao, K., Stephanou, H. E., "Optimal Placement of Microactuators for Distributed Control using Neural Networks", Chapter in Recent

Advances in Control Systems, Robotics, and Automation, 2 ed., edited by S. Pennacchio, pp. 29-36, International SAR, Palermo, Italy, 2008.

[27] S. Floyd, C. Pawashe, and M. Sitti, “An Untethered MagnaticallyActuated Micro-Robot Capable of Motion on Arbitrary Surfaces”, IEEE Int. Conf. on Robotics and Automation, pp. 419-424, May. 2008.

[28] Ljung, L., and T. Glad. Modeling of Dynamic Systems. PTR Prentice Hall, Upper Saddle River, NJ, 1994.

[29] Ljung, L. System Identification: Theory for the User. Second edition. PTR Prentice Hall, Upper Saddle River, NJ, 1999.

[30] Söderström, T., and P. Stoica. System Identification. Prentice Hall International, London, 1989.

[31] Pintelon, R., and J. Schoukens. System Identification. A Frequency Domain Approach. Wiley-IEEE Press, New York, 2001.

[32] O Nelles, “NON LINEAR SYSTEM IDENTIFICATION”, Springer, 2001. ISBN 3-540-67369-5.

[33] Diller, Eric; Ye, Zhou; Sitti, Metin, “Rotating magnetic micro-robots for versatile non-contact fluidic manipulation of micro-objects”, Intelligent Robots and Systems (IROS), 2011 IEEE/RSJ International Conference.

[34] Dan O. Popa , Byoung Hun Kangt, John T. Went, Harry E. Stephanou, George Skidmore, Aaron Geisberge, “Dynamic Modeling and Input Shaping of Thermal Bimorph MEMS Actuators”, ICRA'11v9.

[35] Muhammed R. Pac, Student Member, IEEE, Dan O. Popa, Member, IEEE. “3-DOF Untethered Microrobot Powered by a Single Laser Beam Based on Differential Thermal Dynamics”, ICRA'11v9.

[36] Baglio, S.; Castorina, S.; Fortuna, L.; Savalli, N., “Technologies and architectures for autonomous "MEMS" microrobots”, Circuits and Systems, 2002. ISCAS 2002. IEEE International Symposium.

[37] Baglio, S.; Castorina, S.; Fortuna, L.; Savalli, N., “Development of autonomous, mobile micro electro-mechanical devices”, Circuits and Systems, 2002. ISCAS 2002. IEEE International Symposium.

[38] S. Fatikow, U. Rembold, “Microsystem Technology and Microrobotics”, Springer-Verlag, 1997, ISBN: 3-540-605658-0.

[39] J.A. Pelesko, D. H. Bernstein, “Modeling MEMS and NEMS”, Chapman & Hall/CRC Press, 2003ISBN: 1-59488-306-5.

[40] Michel, F.; Ehrfeld, W. “Mechatronic micro devices” Micromechatronics and Human Science, 1999. MHS '99. Proceedings of 1999 International Symposium.

[41] Pakkratok, M.; Luekiatphaisan, N.; Aoyama, H. “Combination of VCA based micro force generator and micro robot for micro hardness and stiffness test”, SICE Annual Conference 2010, Proceedings of Publication Year: 2010 , Page(s): 3184 – 3189.

[42] Mizoguchi, H.; Ando, M.; Mizuno, T.; Takagi, T.; Nakajima, N., “Design and fabrication of light driven micropump”, Micro Electro Mechanical Systems, 1992, MEMS '92, Proceedings. An Investigation of Micro Structures, Sensors, Actuators, Machines and Robot, IEEE.

BIOGRAPHICAL INFORMATION

Sai Kalyan, Yelike was born in India. He completed his Bachelors in Electronics and Computers Engineering from Koneru Lakshmaiah College of Engineering in A.P., INDIA in 2006. He has 3 years of work experience as Modeling and Simulations Engineer. He received his M.S. degree in Electrical Engineering from University of Texas at Arlington in 2012 with specialization in Control Systems and Signal Processing.